Interaction between Hormone-Sensitive Lipase and ChREBP in Fat Cells Controls Insulin Sensitivity

Pauline Morigny, Marianne Houssier, Aline Mairal, Claire Ghilain, Etienne Mouisel, Fadila Benhamed, Bernard Masri, Emeline Recazens, Pierre-Damien Denechaud, Geneviève Tavernier, et al.

1   Interaction between Hormone-Sensitive Lipase and ChREBP in Fat Cells

2   Controls Insulin Sensitivity

3

4   Pauline Morigny[1,2,26], Marianne Houssier[1,2,26], Aline Mairal[1,2], Claire Ghilain[1,2], Etienne

5   Mouisel[1,2], Fadila Benhamed[3,4,5], Bernard Masri[1,2], Emeline Recazens[1,2], Pierre-Damien

6   Denechaud[1,2], Geneviève Tavernier[1,2], Sylvie Caspar-Bauguil[1,2,6], Sam Virtue[7], Veronika

7   Sramkova[1,2,8,9], Laurent Monbrun[1,2], Anne Mazars[1,2], Madjid Zanoun[1,2], Sandra Guilmeau[3,4,5],

8   Valentin Barquissau[1,2], Diane Beuzelin[1,2], Sophie Bonnel[1,2,9], Marie Marques[1,2,9], Boris

9   Monge-Roffarello[1,2], Corinne Lefort[1,2], Barbara Fielding[10], Thierry Sulpice[11], Arne Astrup[12],

10 Bernard Payrastre[1,2], Justine Bertrand-Michel[1,2], Emmanuelle Meugnier[13], Laetitia Ligat[14],

11 Frédéric Lopez[14], Hervé Guillou[15,16], Charlotte Ling[17], Cecilia Holm[18], Remi Rabasa-

12 Lhoret[19,20,21], Wim H. M. Saris[22], Vladimir Stich[8,9], Peter Arner[23], Mikael Rydén[23], Cedric

13 Moro[1,2,9], Nathalie Viguerie[1,2,9], Matthew Harms[24], Stefan Hallén[24], Antonio Vidal-Puig[7,25],

14 Hubert Vidal[13], Catherine Postic[3,4,5], Dominique Langin[1,2,6,9*]

15

16 [1] Institut National de la Santé et de la Recherche Médicale (Inserm), UMR1048, Institute of

17 Metabolic and Cardiovascular Diseases, Toulouse, France;

18 [2] University of Toulouse, UMR1048, Institute of Metabolic and Cardiovascular Diseases,

19 Paul Sabatier University, Toulouse, France;

20 [3] Institut National de la Santé et de la Recherche Médicale (Inserm), U1016, Institut Cochin,

21 Paris, France;

22 [4] Centre National de la Recherche Scientifique (CNRS), UMR 8104, Paris, France;

23 [5] Université Paris Descartes, Sorbonne Paris Cité, Paris, France;

24 [6] Toulouse University Hospitals, Laboratory of Clinical Biochemistry, Toulouse, France;

25   [7] University of Cambridge Metabolic Research Laboratories, Wellcome Trust-MRC Institute

26   of Metabolic Science, Addenbrooke's Hospital, Cambridge CB2 0QQ, UK;

27   [8] Department for the Study of Obesity and Diabetes, Third Faculty of Medicine, Charles

28   University, Prague, Czech Republic;

29   [9] Franco-Czech Laboratory for Clinical Research on Obesity, Third Faculty of Medicine,

30   Prague and Paul Sabatier University, Toulouse, France;

31   [10] Department of Nutritional Sciences, University of Surrey, Guildford, Surrey;

32   [11] Physiogenex SAS, Prologue Biotech, Labège, France;

33   [12] Department of Nutrition, Exercise and Sports, Faculty of Science, University of

34   Copenhagen, Copenhagen, Denmark;

35   [13] CarMeN Laboratory, Inserm U1060, INRA U1397, Université Lyon 1, INSA Lyon,

36   Oullins, France;

37   [14] Pôle Technologique, Cancer Research Center of Toulouse (CRCT), Plateau Interactions

38   Moléculaires, INSERM-UMR1037, 31037 Toulouse, France.

39   [15] Institut National de la Recherche Agronomique (INRA), UMR1331, Integrative Toxicology

40   and Metabolism, Toulouse, France

41   [16] University of Toulouse, UMR1331, Institut National Polytechnique (INP), Paul Sabatier

42   University, Toulouse, France;

43   [17] Department of Clinical Sciences, Epigenetics and Diabetes, Lund University Diabetes

44   Centre, Clinical Research Centre, Malmö, Sweden;

45   [18] Department of Experimental Medical Science, Lund University, Biomedical Centre, Lund,

46   Sweden;

47   [19] Institut de Recherches Cliniques de Montréal, Montreal, Canada;

48   [20] Department of nutrition, Université de Montréal, Montreal, Canada;

49   [21] Montreal Diabetes Research Center (MDRC), Montreal, Canada;

50 [22] Department of Human Biology, NUTRIM School of Nutrition and Translational Research

51 in Metabolism, Maastricht University Medical Centre, Maastricht, Netherlands;

52 [23] Department of Medicine, H7 Karolinska Institutet and Karolinska University Hospital,

53 Huddinge, Stockholm, Sweden;

54 [24] Cardiovascular, Renal and Metabolism, IMED Biotech Unit, AstraZeneca, Gothenburg,

55 Sweden;

56 [25] Wellcome Trust Sanger Institute, Wellcome Trust Genome Campus, Hinxton,

57 Cambridgeshire CB10 1SA, UK;

58 [26] These authors contributed equally to the work.

59

60 *e-mail : dominique.langin@inserm.fr

61

62 ABSTRACT

63 Impaired adipose tissue insulin signaling is a critical feature of insulin resistance. Here we

64 identify a pathway linking the lipolytic enzyme, hormone-sensitive lipase (HSL), to insulin

65 action via the glucose-responsive transcription factor ChREBP and its target, the fatty acid

66 (FA) elongase, ELOVL6. Genetic inhibition of HSL in human adipocytes and mouse adipose

67 tissue results in enhanced insulin sensitivity and induction of ELOVL6. ELOVL6 promotes an

68 increase in phospholipid (PL) oleic acid which modifies plasma membrane fluidity and

69 enhances insulin signaling. HSL deficiency-mediated effects are suppressed by gene silencing

70 of ChREBP and ELOVL6. Mechanistically, physical interaction between HSL and

71 ChREBPα, independently of lipase catalytic activity, impairs ChREBPα translocation into the

72 nucleus and induction of ChREBPβ, the transcriptionally highly active isoform strongly

73 associated to whole body insulin sensitivity. Targeting the HSL-ChREBP interaction may

74 allow therapeutic strategies for the restoration of insulin sensitivity.

75

Introduction

Insulin resistance is a pathogenic mechanism involved in a wide array of diseases. Besides the well-established early defect seen in type 2 diabetes, insulin resistance plays a role in the development of cancers such as colorectal cancer, liver diseases associated with non-alcoholic steatohepatitis, cardiovascular diseases or, reproductive dysfunction e.g., in polycystic ovary syndrome. Insulin resistance is also a feature of aging-related disorders such as neurodegenerative diseases e.g., in Alzheimer disease. Adipose tissue metabolism has emerged as a major determinant of systemic insulin sensitivity. Genetic ablation of insulin-induced glucose transport in fat causes systemic insulin resistance [1]. Direct manipulation of the fat cell insulin signaling pathway in mice also supports the systemic importance of adipose tissue [2-4]. Defects in adipose insulin signaling have been reported in insulin resistant and type 2 diabetic patients [5-8]. In this context, improvement of adipose tissue insulin action appears to be an important target for recovery of whole body systemic insulin sensitivity. Glitazones, a well-known class of insulin sensitizers, act through modulation of fat cell insulin sensitivity [9,10]. Given their side-effects and subsequent withdrawal in many countries, there is an unmet need of drugs targeting adipose tissue. Excessive circulating levels of fatty acids are considered as important contributors to insulin resistance through development of fatty acid-induced lipotoxicity in insulin-sensitive tissues such as liver and skeletal muscle [11]. Lowering of plasma non-esterified fatty acid levels through inhibition of fat cell lipolysis has been proposed as an approach to improve insulin sensitivity. However, human data questions the association between production of fatty acids from adipose tissue lipolysis and insulin resistance in obesity [12]. Partial deficiency in HSL (encoded by *LIPE*), one of the neutral lipases expressed in adipocytes, results in improvement of whole body insulin sensitivity in obese mice without changes in plasma fatty acid levels suggesting that other mechanisms than lipolysis are involved [13].

101 Here, in a series of in vitro and in vivo studies in humans and mice, we identified a pathway

102 linking HSL to insulin resistance through interaction with the glucose-responsive transcription

103 factor ChREBP. The physical interaction between HSL and ChREBP impairs nuclear

104 translocation and activity of the transcription factor. In fat cells, the lipogenic enzyme

105 ELOVL6 is a preferential target of ChREBP. Inhibition of HSL promotes activity of ELOVL6

106 and enhances insulin signaling through enrichment of plasma membrane phospholipids in

107 oleic acid.

108

109 **Reduction in HSL expression promotes *de novo* lipogenesis and insulin signaling in**

110 **human adipocytes**

111 In adipocytes differentiated from human multipotent adipose-derived stem (hMADS) cells

112 [14,15], HSL gene silencing (**Supplementary Fig. 1a,b,c**) increased insulin-stimulated glucose

113 transport (**Fig. 1a**), glucose oxidation (**Fig. 1b**) and glucose carbon incorporation into FA, i.e.

114 *de novo* lipogenesis (**Fig. 1c**). Insulin signaling was enhanced in adipocytes with decreased

115 HSL expression as shown by enhanced activating phosphorylations of insulin receptor

116 substrate 1 (IRS1-pY612) and V-Akt murine thymoma viral oncogene homolog

117 (AKT)/protein kinase B (AKT-pS473, AKT-pT308) after insulin treatment (**Fig. 1d,e,f**).

118 Phosphorylation of AS160, an AKT substrate regulating translocation of the insulin-sensitive

119 glucose transporter GLUT4, showed a trend similar to IRS1 and AKT phosphorylation (**Fig.**

120 **1g**). As adipose tissue *de novo* lipogenesis is associated with insulin sensitivity in humans

121 [16,17], we tested whether direct inhibition of *de novo* lipogenesis has an impact on the

122 modulation of insulin signaling induced by HSL depletion. To this end, human adipocytes

123 were treated with a selective inhibitor of FA synthase, the rate-limiting enzyme in the

124 synthesis of palmitic acid (**Supplementary Fig. 1d**). The FA synthase inhibitor blunted the

125 induction of insulin-mediated phosphorylation of AKT observed in HSL-deficient fat cells

126   (**Supplementary Fig. 1e**). To further probe the role of *de novo* lipogenesis, we analyzed FA

127   composition in fat cell triglycerides (TG) and PL. HSL inhibition significantly decreased the

128   proportion of palmitic acid and palmitoleic acid but increased that of oleic acid in TG and PL

129   (**Fig. 1h,i**).

130   To define the molecular mechanisms underlying the changes in FA composition, we analyzed

131   gene expression of enzymes catalyzing key steps in the synthesis of the main saturated and

132   monounsaturated FA derived from glucose in human fat cells (**Supplementary Fig. 1d**). In

133   hMADS adipocytes with decreased HSL expression, the most robust induction was observed

134   for *ELOVL6* (**Fig. 1j**). The increase in *ELOVL6* mRNA level was mirrored by an increase in

135   enzyme activity (**Supplementary Fig. 1f**) and an increase in the FA elongation ratio

136   attributable to ELOVL6 activity (**Supplementary Fig. 1g**). To confirm data from hMADS

137   adipocytes, we performed HSL gene silencing in human preadipocytes differentiated in

138   primary cultures. *ELOVL6* also showed the highest induction among *de novo* lipogenesis

139   genes (**Supplementary Fig. 1h**). Next, we evaluated the effect of adipose triglyceride lipase

140   (ATGL encoded by *PNPLA2*), through ATGL gene silencing in hMADS adipocytes

141   (**Supplementary Fig. 1i,j**). ATGL precedes HSL in the sequential breakdown of TG during

142   adipocyte lipolysis. Contrarily to what is observed during HSL depletion, ATGL knock down

143   had no effect on *ELOVL6* and other *de novo* lipogenic enzyme mRNA levels as well as on the

144   FA elongation ratio attributable to ELOVL6 activity (**Supplementary Fig. 1k,l**). Altogether,

145   the results show that HSL depletion improves insulin signaling and, promotes *de novo*

146   lipogenesis and modification in FA composition. These changes are associated with induction

147   of the FA elongase ELOVL6.

148

149   **HSL inhibition is associated with improved insulin sensitivity and increased adipose**

150   **tissue *Elovl6* expression in vivo**

151   To probe changes in insulin sensitivity upon decreased HSL expression in vivo, we

152   investigated different mouse transgenic models, genetic backgrounds and diets. First, we

153   investigated B6D2/F1 transgenic mice with *Lipe* haploinsufficiency fed with 60% high fat

154   diet [13]. Compared to obese wild type littermates, the mice showed no differences in body

155   weight and fat mass (**Supplementary Fig. 2a,b**). During euglycemic hyperinsulinemic clamp,

156   the glucose infusion rate tended to increase (**Fig. 2a**) while there was no change in glucose

157   rate of disappearance in obese *Lipe* haploinsufficient mice compared with wild type

158   littermates (**Fig. 2b**). Insulin-mediated suppression of hepatic glucose production was

159   improved (**Fig. 2c**). In a second cohort of B6D2/F1 mice fed 45% high fat diet, insulin

160   tolerance was improved while body weight was not modified in *Lipe* haploinsufficient mice

161   compared with wild type littermates (**Fig. 2d, Supplementary Fig. 2c**). In a third cohort of

162   C57BL/6J mice fed 60% high fat diet, we confirmed enhanced insulin sensitivity in *Lipe*

163   haploinsufficient mice as determined by quantitative insulin-sensitivity check index

164   (QUICKI) (**Fig. 2e**). Adipose *Elovl6* gene expression was higher in mice with diminished

165   HSL expression (**Fig. 2f**). As in human adipocytes (**Fig. 1j, Supplementary Fig 1h**), the

166   induction was more pronounced for *Elovl6* than for other lipogenic genes (**Supplementary**

167   **Fig. 2d**).

168   To generate a mouse model with HSL knock down in adipose tissue and unaltered expression

169   in liver, we produced B6D2/F1 mice with zinc finger nuclease-mediated deletion of exon B

170   (**Supplementary Fig. 2e**). The promoter upstream of exon B governs HSL expression in fat

171   cells [18]. *Lipe*^exonB-/-^ mice showed decreased expression of HSL in adipose tissue (**Fig. 2g,h**). In

172   liver, the low levels of HSL which are mainly composed of exon A-containing transcripts,

173   were not modified (**Supplementary Fig. 2f,g**). *Lipe*^exonB-/-^ mice fed high fat diet showed

174   improved glucose tolerance (**Fig. 2i**) without alteration of body weight (**Supplementary Fig.**

175   **2h**). Adipose *Elovl6* gene expression was higher in these mice compared to wild type

176 littermates (**Fig. 2j**). Pharmacological inhibition of HSL had positive effect in C57BL/6J

177 mice. Chronic treatment with a specific inhibitor of HSL did not alter body weight

178 (**Supplementary Fig. 2i**) but resulted in increased QUICKI (**Supplementary Fig. 2j**) and

179 higher induction of adipose *Elovl6* gene expression (**Supplementary Fig. 2k**). Therefore,

180 both genetic and pharmacologic inhibition of HSL results in improved insulin sensitivity and

181 enhanced *Elovl6* expression in adipose tissue in vivo.

182
183 **Adipose ELOVL6 has a positive effect on insulin signaling and is associated with insulin**

184 **sensitivity in vitro and in vivo**

185 To determine whether ELOVL6 was involved in the improvement of insulin signaling when

186 fat cell HSL expression is diminished, we performed siRNA-mediated knockdown of

187 ELOVL6 in human adipocytes. Gene silencing led to a significant decrease in *ELOVL6*

188 mRNA level and activity (**Supplementary Fig. 3a,b**). The increases in IRS1 (**Fig. 3a**) and

189 AKT (**Fig. 3b, Supplementary Fig. 3c**) phosphorylation observed in HSL-deficient

190 adipocytes were abrogated following concomitant gene silencing of ELOVL6. To assess the

191 importance of Elovl6 on adipose tissue insulin signaling in vivo, a bolus of insulin was

192 injected to wild type and *Elovl6* null mice of similar body weights prior to collection and

193 analyses of fat pads (**Supplementary Fig. 3d,e**). In agreement with in vitro data in human

194 adipocytes, insulin-stimulated Akt phosphorylation was decreased in adipose tissue of *Elovl6*

195 null mice (**Fig. 3c**). These results reveal a strong link between ELOVL6 and insulin signaling

196 in fat cells and identify ELOVL6 as the mediator of the beneficial effects of HSL inhibition.

197 The relationship between adipose tissue ELOVL6 and insulin sensitivity was further explored

198 in mouse models and clinical cohorts. In mice fed high fat diet, the C57BL/6J strain showed

199 higher insulin tolerance than DBA/2J strain (**Fig. 3d, Supplementary Fig. 3f**). The better

200 insulin action in C57BL/6J mice was accompanied by higher induction of adipose tissue

201 *Elovl6* gene expression during refeeding (**Fig. 3e**). In humans, *ELOVL6* gene expression was

202   first measured in visceral adipose tissue from lean insulin-sensitive individuals and obese

203   patients with metabolic syndrome, the latter being characterized by higher body mass index

204   and lower glucose disposal rate measured during euglycemic hyperinsulinemic clamp (**Fig. 3f,**

205   **Supplementary Fig. 3g**). Adipose tissue *ELOVL6* mRNA levels were lower in insulin

206   resistant individuals (**Fig. 3g**). Additional evidence was provided by a longitudinal study. In

207   morbidly obese subjects, the weight loss observed two years after bariatric surgery

208   (**Supplementary Fig. 3h**) was associated with an improvement in insulin sensitivity

209   estimated by euglycemic hyperinsulinemic clamp-derived M value (**Fig. 3h**) and an increase

210   in subcutaneous adipose *ELOVL6* mRNA level (**Fig. 3i**). A strong positive correlation was

211   found between *ELOVL6* mRNA levels in subcutaneous fat and M value (**Supplementary Fig.**

212   **3i**). Taken together, both murine and human data show a positive association between adipose

213   *ELOVL6* expression and insulin sensitivity in vivo.

214

215   **ELOVL6 positive effect on insulin signaling is mediated by oleic acid content in PL and**

216   **plasma membrane fluidity**

217   We sought to identify the mechanisms by which ELOVL6 improves insulin signaling.

218   Considering that the enzyme catalyzes critical steps in FA synthesis (**Supplementary Fig.**

219   **1d**), we investigated the direct contribution of ELOVL6 on the changes in fat cell FA

220   composition. In TG (**Fig. 4a**) and PL (**Fig. 4b**) of human adipocytes, diminished ELOVL6

221   expression led to an increase in palmitic acid and palmitoleic acid at the expense of oleic acid.

222   Analyses of these FAs were then performed on each class of PL. ELOVL6-deficient

223   adipocytes showed a decrease in the proportion of oleic acid (e.g., 36:2) and an increase in the

224   proportion of palmitic acid (e.g., 32:0) and palmitoleic acid (e.g., 32:2) in

225   phosphatidylcholines and phosphatidylethanolamines (**Supplementary Fig. 4a-d**). In

226   phosphatidylinositides, there was a decrease in 36:2 whereas no change was observed for

227   phosphatidylserines. These findings were in agreement with in vivo data, where the lack of

228   *Elovl6* in mouse adipose tissue resulted in increased palmitic and palmitoleic acid and

229   decreased oleic acid contents in adipose tissue (**Supplementary Fig. 4e**). The changes in FA

230   composition of PL suggest potential modification in plasma membrane properties. As

231   ELOVL6 mediates the positive effect of HSL gene silencing on insulin signaling (**Fig. 3a,b,**

232   **Supplementary Fig. 3c**), we determined whether this effect was dependent on oleic acid.

233   There are two enzymatic steps between palmitic acid and oleic acid (**Supplementary Fig.**

234   **1d**). The first is the elongation of palmitic acid into stearic acid catalyzed by ELOVL6 and the

235   second is the desaturation of stearic acid into oleic acid catalyzed by SCD, a highly active

236   process in fat cells [19-22]. To investigate the respective contribution of the two steps, specific

237   inhibitors were used. Treatment of human adipocytes with an inhibitor of ELOVL6 [23] resulted

238   in the expected changes in FA composition with a decrease of the C18/C16 FA ratio (**Fig. 4c**).

239   Concordant with data obtained using gene silencing (**Fig. 3b**), pharmacological inhibition of

240   ELOVL6 abrogated the enhancement of insulin-induced AKT phosphorylation observed in

241   HSL-deficient adipocytes (**Fig. 4d**). A specific SCD inhibitor [24] decreased C16 and C18 FA

242   desaturation (**Fig. 4e**) and had the same effect as the ELOVL6 inhibitor on AKT

243   phosphorylation (**Fig. 4f**). Our data suggest that SCD is necessary but does not play a rate-

244   limiting role as does ELOVL6 in the improvement of insulin signaling induced by HSL

245   inhibition. Accordingly, *SCD* mRNA levels are much higher than *ELOVL6* mRNA levels in

246   human adipocytes (**Supplementary Fig. 4f**). In additional experiments, the content of oleic

247   acid in PL was directly modified by incubation of adipocytes with the FA (**Fig. 4g**). Exposure

248   of HSL and ELOVL6 double deficient adipocytes to oleic acid rescued insulin-induced AKT

249   phosphorylation to levels comparable with that observed in fat cells with diminished HSL

250   expression (**Fig. 4h**). Therefore, the beneficial role of ELOVL6 on insulin signaling in human

251   adipocytes is mediated by modulation of oleic acid content.

252   The composition of FA in PL may influence insulin signal transduction through modification

253   of plasma membrane properties [19,25,26]. To determine the consequence of ELOVL6-mediated

254   changes in PL FA composition on plasma membrane fluidity, overexpression of ELOVL6 in

255   human adipocytes was achieved using an adenoviral vector (**Supplementary Fig. 4g,h**). The

256   resulting increase in C18/C16 FA ratio (**Fig. 4i**) was associated with an increase in insulin-

257   induced IRS1 phosphorylation (**Fig. 4j**). Fluorescence recovery after photobleaching (FRAP)

258   data were analyzed in cells overexpressing ELOVL6 which plasma membrane glycolipids

259   were labeled by fluorescent cholera toxin subunit B (**Fig. 4k**). Comparison of the mobile

260   fractions (**Fig. 4l**) revealed an increase in plasma membrane lateral mobility of cholera toxin-

261   bound glycolipids in ELOVL6-overexpressing adipocytes. Collectively, the data suggest that

262   enhanced adipocyte ELOVL6 activity increases the proportion of oleic acid in PL and

263   positively influences insulin signaling through modulation of plasma membrane fluidity.

264

265   **The glucose-responsive transcription factor ChREBP mediates the beneficial effect of**

266   **diminished HSL expression through ELOVL6 induction**

267   ELOVL6 is a direct transcriptional target of ChREBP [27]. Adipose ChREBP is a major

268   determinant of systemic insulin action on glucose metabolism [28]. Therefore, the direct

269   contribution of ChREBP to HSL gene silencing-mediated improvement of glucose

270   metabolism in human adipocytes was evaluated using RNA interference (**Supplementary**

271   **Fig. 5a**). During dual knockdown of HSL and ChREBP, the beneficial effects on glucose

272   metabolism observed in adipocytes with low HSL expression were diminished. Glucose

273   transport was decreased to control levels and the induction of *de novo* lipogenesis observed in

274   cells with single HSL knockdown was lowered in adipocytes with dual knockdown of HSL

275   and ChREBP (**Fig. 5a,b**). A similar pattern was observed for glucose and acetate carbon

276   incorporation into FA (**Fig. 5b,c**) showing that the upregulation of FA synthesis resulted not

277   only from increased glucose uptake but also from specific induction of *de novo* lipogenesis.

278   ChREBP gene silencing also mitigated the increase in insulin-induced IRS1 and AKT

279   phosphorylation (**Fig. 5d,e**). These results indicate that ChREBP is involved in the

280   improvement of glucose metabolism and insulin signaling induced by HSL downregulation.

281   Similarly to what had been observed for ELOVL6 knock down (**Fig. 4a,b**), ChREBP gene

282   silencing led to an increase in palmitic acid and palmitoleic acid and a decrease of oleic acid

283   (**Fig. 5f,g**). Accordingly, ChREBP gene silencing potently suppressed *ELOVL6* gene

284   expression but had weak or no effect on other lipogenic genes suggesting that ELOVL6 is a

285   preferential target of ChREBP in human fat cells (**Fig. 5h**). The involvement of ChREBP in

286   adipose *Elovl6* gene expression was confirmed in vivo. In adipose tissue of *Mlxipl* null mice

287   (**Supplementary Fig. 5b**), *Elovl6* was the lipogenic gene which expression was the most

288   severely impaired (**Fig. 5i**).

289   Two isoforms of ChREBP have been identified. ChREBPα, which transcriptional activity is

290   regulated by glucose, and ChREBPβ, a transcriptionally superactive and unstable isoform

291   which is a direct transcriptional target of ChREBPα [28,29]. We characterized the human β-

292   specific exon of *MLXIPL* which extends 29 deoxynucleotides 3' of its mouse counterpart [28]

293   (**Supplementary Fig. 5c**). In human adipocytes with siRNA-mediated knock down of HSL,

294   the levels of *ChREBP* transcripts, notably the β isoform, were increased (**Fig. 5j**).

295   Recruitment of ChREBP on the functional carbohydrate response element (ChoRE) in the

296   *ELOVL6* promoter was investigated using chromatin immunoprecipitation assays [27]. In

297   hMADS adipocytes, more binding events were detected on the *ELOVL6* ChoRE than on

298   positive control regions in *RORC* and *TXNIP*, a well characterized target of ChREBP

299   (**Supplementary Fig. 5d**). ChREBP recruitment onto the *ELOVL6* promoter was markedly

300   enhanced in HSL-deficient compared to control adipocytes (**Fig. 5k**).

301   Interestingly, *ELOVL6* was strongly associated with *ChREBPβ* gene expression in human

302   hMADS adipocytes (**Fig. 5l**) and human differentiated primary preadipocytes

303   (**Supplementary Fig. 5e**). Albeit less potent, a positive correlation was also found between

304   *ELOVL6* and *ChREBPα* (**Supplementary Fig. 5f**). Similarly, a highly significant correlation

305   between *ELOVL6* and *ChREBPβ* was observed in human subcutaneous adipose tissue

306   samples (**Fig. 5m**). Short term elevation in plasma glucose and insulin levels during a

307   hyperglycemic hyperinsulinemic clamp led to a pronounced induction of adipose *ChREBPβ*

308   (**Fig. 5n**) and *ELOVL6* (**Fig. 5o**) gene expression, illustrating the importance of glucose flux

309   into the fat cells in the control of *ELOVL6* expression in humans. Altogether, our results show

310   that ChREBPβ mediates the effect of HSL deficiency on glucose metabolism and insulin

311   signaling through transcriptional activation of *ELOVL6*.

312

313   **HSL modifies ChREBP activity in fat cells through protein-protein interaction**

314   As HSL catalyzes one of the rate-limiting steps in fat cell TG hydrolysis, we investigated

315   whether lipolysis per se contributed to the induction of ChREBP. Several lines of evidence

316   suggest that this is not the case. In the culture conditions used to study *de novo* lipogenesis,

317   the release of glycerol and FA in the culture medium was low and was not influenced by HSL

318   gene silencing (**Supplementary Fig. 6a,b**). Adipocytes were then treated with triacsin C, a

319   potent inhibitor of long chain fatty acyl CoA synthetase [14]. If FAs were involved, enhanced

320   FA levels due to blockade of FA re-esterification should influence *ChREBP* and *ELOVL6*

321   induction in adipocytes with HSL knock down. However, the upregulation of *ChREBP*

322   isoform and *ELOVL6* mRNA was not influenced by the treatment (**Supplementary Fig. 6c-**

323   **e**). These data show that the lipolytic activity of HSL does not contribute to the induction of

324   ChREBP.

325　These findings led us to hypothesize that physical interaction between HSL and ChREBP may

326　influence ChREBP activity. HEK293 cells were transfected with vectors expressing HSL and

327　ChREBPα with FLAG epitope tag [30]. Immunoprecipitation of cell lysates with anti-FLAG

328　IgG and immunoblotting with anti-HSL antibody showed that HSL co-immunoprecipitated

329　with ChREBPα (**Supplementary Fig. 6f**). Co-immunoprecipitation was observed using

330　FLAG-ChREBP immobilized on magnetic beads and recombinant HSL (**Fig. 6a**). Surface

331　plasmon resonance assays supported a direct binding between ChREBPα and HSL (**Fig. 6b**).

332　Interaction between endogenous proteins in adipocytes was shown through

333　immunoprecipitation with anti-ChREBP and anti-HSL antibodies (**Fig. 6c, Supplementary**

334　**Fig. 6g**). In line with the lack of effect on *de novo* lipogenesis (**Supplementary Fig. 1k,l**),

335　ATGL displayed no interaction with ChREBPα further indicating that HSL interaction with

336　ChREBPα is independent lipolysis and specific to this neutral lipase (**Fig. 6c**).

337　Furthermore, interaction of HSL with ChREBPα was shown using in situ proximity ligation

338　assays using a pair of primary antibodies raised in two different species and a pair of

339　secondary antibodies coupled to oligodeoxynucleotides [31]. Specific and robust fluorescence

340　signals were observed in the cytosol of fat cells from subcutaneous adipose tissue

341　(**Supplementary Fig. 6h**). Such signals were also seen in differentiated hMADS adipocytes

342　(**Supplementary Fig. 6i**). Little signal was detected in undifferentiated fibroblasts which do

343　not express HSL. Negative controls using incomplete sets of antibodies and assays using anti-

344　ATGL and anti-AKT combined with anti-ChREBP antibodies supported specificity of the

345　interaction (**Supplementary Fig. 6j,k**). Human HepG2 hepatocytes which express significant

346　level of ChREBP but minute amounts of HSL showed few fluorescent spots (**Supplementary**

347　**Fig. 6l,m**). Respective expression of ChREBPα and HSL in mouse tissues is coherent with a

348　fat-specific interaction of the two proteins (**Supplementary Fig. 6n**). The data suggest that

349　ChREBPα interaction with HSL is specific to fat cells.

350   In mouse adipose tissue, co-immunoprecipitation between HSL and ChREBP was diminished

351   in *Lipe* haploinsufficient mice (**Fig. 6d**). In human adipocytes, HSL binding to ChREBPα was

352   reduced in cytoplasm when HSL expression was diminished using siRNA (**Fig. 6e,**

353   **Supplementary Fig. 7a**). This resulted in modification of ChREBP cellular distribution.

354   Compared to control cells, adipocytes with low HSL expression showed higher

355   immunofluorescence of ChREBP in nuclei indicating that ChREBPα nuclear translocation is

356   facilitated when interaction with HSL is diminished (**Fig. 6f**). Subcellular fractionation

357   confirmed an increased nuclear translocation in human adipocytes and mouse adipose tissues

358   with low HSL expression whereas no significant differences was observed in the cytosolic

359   fraction (**Fig. 6g,h, Supplementary Fig. 7b,c**). In mice, there was no difference in ChREBPα

360   protein content in fat pads of the two genotypes (**Supplementary Fig. 7d**). To evaluate the

361   effect of HSL on ChREBPα transcriptional activity, HEK293 cells were transfected with a

362   vector containing the luciferase reporter gene under the control of a promoter containing

363   functional ChoREs [32]. Promoter activity increased when cells expressed ChREBPα and

364   decreased when cells co-expressed increasing amounts of HSL (**Fig. 6i, Supplementary Fig.**

365   **7e**). The data suggest that HSL binds to ChREBPα and sequesters the transcription factor in

366   the cytoplasm. Upon decrease of HSL expression, HSL-ChREBP interaction is diminished,

367   ChREBPα nuclear translocation is facilitated and its transcriptional activity is enhanced as

368   shown here in reporter gene assays and above in chromatin immunoprecipitation analysis

369   (**Fig. 5k**).

370   When HEK293 cells expressing HSL and ChREBP were treated with a HSL inhibitor, less

371   interaction between HSL and ChREBP was observed (**Supplementary Fig. 7f**). In human

372   adipose tissue, we previously identified a short form of HSL produced by in-frame skipping

373   of exon 6 (**Supplementary Fig. 2e**) [33,34]. As exon 6 encodes the catalytic site Serine, HSL

374   short form is devoid of enzymatic activity (**Supplementary Fig. 7g**). Expressed in HEK293

cells, HSL short form retained the capacity to bind ChREBP (**Fig. 6j**). An adenovirus

expressing HSL short form was used to transduce human adipocytes transfected with control

or *LIPE* siRNA (**Supplementary Fig. 7h**). The induction of *ELOVL6* in adipocytes with

diminished levels of HSL was blunted when HSL short form was expressed (**Fig. 6k**). A

similar pattern was observed for other *de novo* lipogenesis gene expression (**Supplementary**

Fig. 7i). The catalytically inactive form also reduced the increase in IRS1 phosphorylation

mediated by HSL down regulation (**Fig. 6l**). Of note, the improvement of fat cell insulin

signaling was observed with no change in amount of ChREBPα protein in adipocytes

expressing HSL-S and in the absence of correlation between HSL and ChREBPα levels.

(**Supplementary Fig. 7j,k**). Altogether, our data suggest that HSL plays an important role

besides the hydrolysis of lipids in fat cells, the repression of ChREBP activity via direct

interaction with the transcription factor (**Supplementary Fig. 8**).

Discussion

Considering the soaring incidence of diseases characterized by an insulin resistance state,

there is a lack of drugs acting on adipose tissue. Its specialized cells, the adipocytes, have

great potential to be therapeutically targeted [35]. Partial inhibition of the fat cell neutral lipase,

HSL, alleviates insulin resistance without increasing body weight, two essential requirements

for therapeutic interventions [13] (and present work). Evolution of plasma fatty acid level and

variation in insulin sensitivity was dissociated in this model. Here, we deciphered the

mechanisms behind HSL inhibition-mediated improvement of glucose metabolism and

identified interactions between prototypical metabolic pathways of the adipocyte. We show

that, independently of lipolysis and the enzyme catalytic activity, HSL physically interacts

with and inhibits the transcription factor ChREBP. ChREBP controls the FA elongase

ELOVL6 catalyzing a limiting step in oleic acid synthesis. The resulting increase in PL oleic

acid content modifies plasma membrane properties and improves insulin signaling.

401   Adipose *de novo* lipogenesis is positively associated with systemic insulin sensitivity [36,37]. *De*

402   *novo* lipogenesis is under the control of the glucose-responsive transcription factor, ChREBP.

403   A positive association between insulin sensitivity and adipose ChREBP, notably, the

404   transcriptionally superactive β isoform, has been reported [16,28,38]. In human adipocytes, we

405   show that knockdown of ChREBP counteracts the beneficial effects of HSL gene silencing on

406   insulin sensitivity. We identify the FA elongase ELOVL6 as the main target of ChREBPβ in

407   HSL-deficient adipocytes. In humans, *ELOVL6* expression in fat was lower in insulin resistant

408   than in insulin sensitive subjects in line with previous reports [16,39]. Of note, in monozygotic

409   twin pairs discordant for type 2 diabetes, adipose *ELOVL6* is markedly lower in the affected

410   twins [40]. Our results from bariatric surgery, a longitudinal intervention improving insulin

411   control of glucose metabolism, also supported the tight link between adipose *ELOVL6* and

412   insulin sensitivity.

413   ELOVL6 catalyzes a critical step in the elongation of C16 FA [22,41]. In adipocytes, enhanced

414   ELOVL6 activity favored oleic acid synthesis while ELOVL6 knock down had the opposite

415   effect. Diets rich in olive oil improve insulin sensitivity at adipocyte and whole-body levels

416   [42,43]. This effect may contribute to the decreased incidence of type 2 diabetes in patients at risk

417   fed Mediterranean diets [43]. At the cellular level, monounsaturated fatty acids have been

418   reported to protect from the damaging effect of palmitic acid on insulin signaling [19,26]. As

419   ELOVL6 induced an increase of oleic acid in major classes of PL, we postulated that it may

420   alter plasma membrane fluidity owing to its conformational plasticity [25,44,45]. The plasma

421   membrane lateral mobility of glycolipids was increased in fat cells overexpressing ELOVL6.

422   We therefore propose that ELOVL6-mediated increase in PL oleic acid content improves fat

423   cell insulin signaling through alteration of plasma membrane properties. In mice, *Elovl6*

424   deficiency impaired white adipose tissue insulin signaling whereas the opposite or lack of

425   alteration have previously been reported in the liver suggesting tissue-specific differences in

426   ELOVL6-mediated modulation of insulin action [41,46].

427   The role of HSL in human fat cell lipolysis is well established [14,47]. HSL is a multifunctional

428   enzyme with a broad range of substrates. Besides tri-, di- and monoglycerides, HSL is able to

429   hydrolyze other esters, such as cholesteryl and retinyl esters [48]. As ChREBP activity is

430   influenced by metabolites and other transcription factors in liver, it could be postulated that

431   products of HSL enzymatic activity directly or indirectly influence ChREBP-mediated

432   modulation of gene transcription [29]. However, although we cannot rule out that, in some

433   conditions, upregulation of ChREBPα protein expression partially contributes to the

434   phenotype of adipocytes depleted in HSL, we bring a solid body of evidence that physical

435   interaction between HSL and ChREBPα controls the intracellular location and activity of the

436   transcription factor in fat cells. ATGL which catalyzes the first step in adipose tissue lipolysis

437   does not interact with ChREBP and does not modulate *de novo* lipogenesis gene expression.

438   Moreover, using a short inactive form of HSL lacking the catalytic site Serine, we could show

439   that the catalytic activity of HSL is dispensable for the interaction with ChREBP and

440   ChREBP-mediated effect on *ELOVL6* expression and insulin signaling. Noteworthy, our data

441   provide a function to this naturally occurring form expressed in human adipose tissue [33]. A

442   specific HSL inhibitor was able to diminish the interaction between HSL and ChREBP and

443   enhance adipose *Elovl6* expression in mice. It may be hypothesized that the inhibitor binding

444   to the catalytic pocket induces conformational change partially disrupting HSL-ChREBP

445   interaction. The data suggest that small molecules may be designed and used to disrupt the

446   interaction. Reducing the interaction between HSL and ChREBP favors ChREBP nuclear

447   translocation and its transcriptional activity. This pathway provides a molecular basis to the

448   differential control of *de novo* lipogenesis in liver and adipose tissue. ChREBP is involved in

449   the regulation of *de novo* lipogenesis in the two tissues [29,49]. However, the pathway is

450   generally considered as detrimental in the liver as it is activated during the development of

451   fatty liver disease whereas it is seen as beneficial in adipose tissue as the link with insulin

452   sensitivity has been shown both in clinical studies and in mouse models [50]. HSL is expressed

453   at much higher level in fat cells than in hepatocytes. Accordingly, interaction between HSL

454   and ChREBP is not found in human hepatocytes. Alleviation of HSL-mediated inhibition of

455   ChREBP activity may constitute a fat cell-specific mechanism to enhance *de novo* lipogenesis

456   and insulin signaling.

457   To conclude, our work identifies a pathway critical for optimal insulin signaling in fat cells

458   which links the neutral lipase HSL to the glucose-responsive transcription factor ChREBP and

459   its target gene, the FA elongase, ELOVL6. This constitutes a unique example of an enzyme

460   involved in lipid metabolism which independently of its enzymatic activity inhibits the

461   transcriptional activity of a glucose-responsive transcription factor through protein-protein

462   interaction. Inhibition of the HSL-ChREBP interaction may constitute an adipose-specific

463   strategy to reduce insulin resistance.

464

480

481   AUTHOR CONTRIBUTIONS

482   P.M. and M.H. share first authorship. P.M. and M.Ho. performed the majority of in vitro

483   experiments and analyzed data with the contribution of A.Mai., C.G., F.B., B.M., E.R.,

484   P.D.D., V.Sr., V.B., D.B., M.M., C.L., L.L., F.L. and M.Ha. P.M., M.Ho., E.Mo., G.T., S.V.,

485   L.M., S.G., B.M.-R., T.S., H.G., C.H., A.V.P. and C.P. performed and analyzed in vivo data

486   from mouse models. P.M., S.B., M.M., B.F., A.A., E.Me., C.L., R.R.L., W.S., V.St., P.A.,

487   M.R., N.V. and H.V. performed and analyzed in vivo data in human clinical studies. S.C.-B.,

488   S.V. and J.B.-M. analyzed lipidomics data. A.Maz. and M.Z. performed and analyzed FRAP

Morigny, Houssier et al.   21

489 experiments. B.P., C.M., N.V., S.H. and H.V. interpreted the data. P.M., M.Ho. and D.L.

490 conceived the study, interpreted the data and wrote the manuscript. D.L. supervised the study.

491

492 COMPETING INTERESTS STATEMENT

493 T.S. is an employee of Physiogenex. M.H. and S.H. are employees of AstraZeneca. The other

494 authors declare no competing financial and non-financial interests.

495

496 REFERENCES

497 1.   Abel, E.D., *et al.* Adipose-selective targeting of the GLUT4 gene impairs insulin

498   action in muscle and liver. *Nature* **409**, 729-733 (2001).

499 2.   Morley, T.S., Xia, J.Y. & Scherer, P.E. Selective enhancement of insulin sensitivity in

500   the mature adipocyte is sufficient for systemic metabolic improvements. *Nat Commun*

501   **6**, 7906 (2015).

502 3.   Shearin, A.L., Monks, B.R., Seale, P. & Birnbaum, M.J. Lack of AKT in adipocytes

503   causes severe lipodystrophy. *Mol Metab* **5**, 472-479 (2016).

504 4.   Softic, S., *et al.* Lipodystrophy Due to Adipose Tissue Specific Insulin Receptor

505   Knockout Results in Progressive NAFLD. *Diabetes* (2016).

506 5.   Rondinone, C.M., *et al.* Insulin receptor substrate (IRS) 1 is reduced and IRS-2 is the

507   main docking protein for phosphatidylinositol 3-kinase in adipocytes from subjects

508   with non-insulin-dependent diabetes mellitus. *Proc Natl Acad Sci U S A* **94**, 4171-

509   4175 (1997).

510 6.   Carvalho, E., Jansson, P.A., Nagaev, I., Wenthzel, A.M. & Smith, U. Insulin

511   resistance with low cellular IRS-1 expression is also associated with low GLUT4

512   expression and impaired insulin-stimulated glucose transport. *FASEB J* **15**, 1101-1103

513   (2001).

514 7.   Frojdo, S., Vidal, H. & Pirola, L. Alterations of insulin signaling in type 2 diabetes: a

515   review of the current evidence from humans. *Biochim Biophys Acta* **1792**, 83-92

516   (2009).

517 8.   Nyman, E., *et al.* A single mechanism can explain network-wide insulin resistance in

518   adipocytes from obese patients with type 2 diabetes. *J Biol Chem* **289**, 33215-33230

519   (2014).

520 9.   Hammarstedt, A., Sopasakis, V.R., Gogg, S., Jansson, P.A. & Smith, U. Improved

521   insulin sensitivity and adipose tissue dysregulation after short-term treatment with

522   pioglitazone in non-diabetic, insulin-resistant subjects. *Diabetologia* **48**, 96-104

523   (2005).

524 10. Yki-Jarvinen, H. Thiazolidinediones. *N Engl J Med* **351**, 1106-1118 (2004).

525 11. Samuel, V.T. & Shulman, G.I. Mechanisms for insulin resistance: common threads

526   and missing links. *Cell* **148**, 852-871 (2012).

527 12. Karpe, F., Dickmann, J.R. & Frayn, K.N. Fatty acids, obesity, and insulin resistance:

528   time for a reevaluation. *Diabetes* **60**, 2441-2449 (2011).

529 13. Girousse, A*., et al.* Partial inhibition of adipose tissue lipolysis improves glucose

530   metabolism and insulin sensitivity without alteration of fat mass. *PLoS Biol* **11**,

531   e1001485 (2013).

532 14. Bezaire, V*., et al.* Contribution of adipose triglyceride lipase and hormone-sensitive

533   lipase to lipolysis in hMADS adipocytes. *J Biol Chem* **284**, 18282-18291 (2009).

534 15. Barquissau, V*., et al.* White-to-brite conversion in human adipocytes promotes

535   metabolic reprogramming towards fatty acid anabolic and catabolic pathways. *Mol*

536   *Metab* **5**, 352-365 (2016).

537 16. Eissing, L*., et al.* De novo lipogenesis in human fat and liver is linked to ChREBP-

538   beta and metabolic health. *Nat Commun* **4**, 1528 (2013).

539 17. Roberts, R*., et al.* Markers of de novo lipogenesis in adipose tissue: associations with

540   small adipocytes and insulin sensitivity in humans. *Diabetologia* **52**, 882-890 (2009).

541 18. Grober, J*., et al.* Characterization of the promoter of human adipocyte hormone-

542   sensitive lipase. *Biochem J* **328**, 453-461 (1997).

543   19.   Collins, J.M., Neville, M.J., Hoppa, M.B. & Frayn, K.N. De novo lipogenesis and

544   stearoyl-CoA desaturase are coordinately regulated in the human adipocyte and

545   protect against palmitate-induced cell injury. *J Biol Chem* **285**, 6044-6052 (2010).

546   20.   Guillou, H., Zadravec, D., Martin, P.G. & Jacobsson, A. The key roles of elongases

547   and desaturases in mammalian fatty acid metabolism: Insights from transgenic mice.

548   *Prog Lipid Res* **49**, 186-199 (2010).

549   21.   Hodson, L. & Fielding, B.A. Stearoyl-CoA desaturase: rogue or innocent bystander?

550   *Prog Lipid Res* **52**, 15-42 (2013).

551   22.   Ohno, Y.*, et al.* ELOVL1 production of C24 acyl-CoAs is linked to C24 sphingolipid

552   synthesis. *Proc Natl Acad Sci U S A* **107**, 18439-18444 (2010).

553   23.   Nagase, T.*, et al.* Synthesis and biological evaluation of a novel 3-sulfonyl-8-

554   azabicyclo[3.2.1]octane class of long chain fatty acid elongase 6 (ELOVL6) inhibitors.

555   *J Med Chem* **52**, 4111-4114 (2009).

556   24.   Xin, Z.*, et al.* Discovery of piperidine-aryl urea-based stearoyl-CoA desaturase 1

557   inhibitors. *Bioorg Med Chem Lett* **18**, 4298-4302 (2008).

558   25.   Antonny, B., Vanni, S., Shindou, H. & Ferreira, T. From zero to six double bonds:

559   phospholipid unsaturation and organelle function. *Trends Cell Biol* **25**, 427-436

560   (2015).

561   26.   Holzer, R.G.*, et al.* Saturated fatty acids induce c-Src clustering within membrane

562   subdomains, leading to JNK activation. *Cell* **147**, 173-184 (2011).

563   27.   Bae, J.S., Oh, A.R., Lee, H.J., Ahn, Y.H. & Cha, J.Y. Hepatic Elovl6 gene expression

564   is regulated by the synergistic action of ChREBP and SREBP-1c. *Biochem Biophys*

565   *Res Commun* **478**, 1060-1066 (2016).

566   28.   Herman, M.A.*, et al.* A novel ChREBP isoform in adipose tissue regulates systemic

567   glucose metabolism. *Nature* **484**, 333-338 (2012).

568   29.   Filhoulaud, G., Guilmeau, S., Dentin, R., Girard, J. & Postic, C. Novel insights into

569   ChREBP regulation and function. *Trends Endocrinol Metab* **24**, 257-268 (2013).

570   30.   Stoeckman, A.K., Ma, L. & Towle, H.C. Mlx is the functional heteromeric partner of

571   the carbohydrate response element-binding protein in glucose regulation of lipogenic

572   enzyme genes. *J Biol Chem* **279**, 15662-15669 (2004).

573   31.   Soderberg, O*., et al.* Direct observation of individual endogenous protein complexes in

574   situ by proximity ligation. *Nat Methods* **3**, 995-1000 (2006).

575   32.   Lou, D.Q*., et al.* Chicken ovalbumin upstream promoter-transcription factor II, a new

576   partner of the glucose response element of the L-type pyruvate kinase gene, acts as an

577   inhibitor of the glucose response. *J Biol Chem* **274**, 28385-28394 (1999).

578   33.   Laurell, H*., et al.* Species-specific alternative splicing generates a catalytically inactive

579   form of human hormone-sensitive lipase. *Biochem J* **328 (Pt 1)**, 137-143 (1997).

580   34.   Ray, H*., et al.* The presence of a catalytically inactive form of hormone-sensitive

581   lipase is associated with decreased lipolysis in abdominal subcutaneous adipose tissue

582   of obese subjects. *Diabetes* **52**, 1417-1422 (2003).

583   35.   Kusminski, C.M., Bickel, P.E. & Scherer, P.E. Targeting adipose tissue in the

584   treatment of obesity-associated diabetes. *Nat Rev Drug Discov* (2016).

585   36.   Czech, M.P. Cellular basis of insulin insensitivity in large rat adipocytes. *J Clin Invest*

586   **57**, 1523-1532 (1976).

587   37.   Hoffstedt, J., Forster, D. & Lofgren, P. Impaired subcutaneous adipocyte lipogenesis

588   is associated with systemic insulin resistance and increased apolipoprotein B/AI ratio

589   in men and women. *J Intern Med* **262**, 131-139 (2007).

590   38.   Kursawe, R*., et al.* Decreased transcription of ChREBP-alpha/beta isoforms in

591   abdominal subcutaneous adipose tissue of obese adolescents with prediabetes or early

Morigny, Houssier et al.   26

592   type 2 diabetes: associations with insulin resistance and hyperglycemia. *Diabetes* **62**,

593   837-844 (2013).

594 39. Soronen, J.*, et al.* Adipose tissue gene expression analysis reveals changes in

595   inflammatory, mitochondrial respiratory and lipid metabolic pathways in obese

596   insulin-resistant subjects. *BMC Med Genomics* **5**, 9 (2012).

597 40. Nilsson, E.*, et al.* Altered DNA methylation and differential expression of genes

598   influencing metabolism and inflammation in adipose tissue from subjects with type 2

599   diabetes. *Diabetes* **63**, 2962-2976 (2014).

600 41. Matsuzaka, T.*, et al.* Crucial role of a long-chain fatty acid elongase, Elovl6, in

601   obesity-induced insulin resistance. *Nat Med* **13**, 1193-1202 (2007).

602 42. Ryan, M.*, et al.* Diabetes and the Mediterranean diet: a beneficial effect of oleic acid

603   on insulin sensitivity, adipocyte glucose transport and endothelium-dependent

604   vasoreactivity. *QJM* **93**, 85-91 (2000).

605 43. Salas-Salvado, J.*, et al.* Reduction in the incidence of type 2 diabetes with the

606   Mediterranean diet: results of the PREDIMED-Reus nutrition intervention randomized

607   trial. *Diabetes Care* **34**, 14-19 (2011).

608 44. Ibarguren, M.*, et al.* Partitioning of liquid-ordered/liquid-disordered membrane

609   microdomains induced by the fluidifying effect of 2-hydroxylated fatty acid

610   derivatives. *Biochim Biophys Acta* **1828**, 2553-2563 (2013).

611 45. Pietilainen, K.H.*, et al.* Association of lipidome remodeling in the adipocyte

612   membrane with acquired obesity in humans. *PLoS Biol* **9**, e1000623 (2011).

613 46. Moon, Y.A., Ochoa, C.R., Mitsche, M.A., Hammer, R.E. & Horton, J.D. Deletion of

614   ELOVL6 blocks the synthesis of oleic acid but does not prevent the development of

615   fatty liver or insulin resistance. *J Lipid Res* **55**, 2597-2605 (2014).

616   47.   Lafontan, M. & Langin, D. Lipolysis and lipid mobilization in human adipose tissue.

617   *Prog Lipid Res* **48**, 275-297 (2009).

618   48.   Kraemer, F.B. & Shen, W.J. Hormone-sensitive lipase: control of intracellular tri-(di-

619   )acylglycerol and cholesteryl ester hydrolysis. *J Lipid Res* **43**, 1585-1594 (2002).

620   49.   Postic, C. & Girard, J. Contribution of de novo fatty acid synthesis to hepatic steatosis

621   and insulin resistance: lessons from genetically engineered mice. *J Clin Invest* **118**,

622   829-838 (2008).

623   50.   Solinas, G., Boren, J. & Dulloo, A.G. De novo lipogenesis in metabolic homeostasis:

624   More friend than foe? *Mol Metab* **4**, 367-377 (2015).

625

FIGURE LEGENDS

627 **Figure 1.** Reduced HSL expression promotes glucose metabolism and insulin signaling in

628 human adipocytes. Experiments were carried out in control (white bars, siCTR) and HSL-

629 deprived (grey bars, siHSL) hMADS adipocytes. (**a-g**) Adipocytes were analyzed in basal (-)

630 and insulin-stimulated (+, 100nM) conditions. (**a**) Glucose transport using radiolabelled 2-

631 deoxyglucose (n=12 biologically independent samples per group) (Insulin stimulation:

632 P<0.0001). (**b**) Glucose oxidation using radiolabelled glucose (n=10 biologically independent

633 samples per group) (Insulin stimulation: P=0.0015). (**c**) *de novo* lipogenesis using

634 radiolabelled glucose (n=10 biologically independent samples per group) (Insulin stimulation:

635 P<0.0001). (**d-g**) Insulin signaling evaluated by activating phosphorylation of IRS1 (pY612)

636 (n=7 biologically independent samples per group) (Insulin stimulation: P=0.0033) (**d**) AKT

637 (pS473) (n=5 biologically independent samples per group) (Insulin stimulation: P=0.0005)

638 (**e**), AKT (pT308) (n=8 biologically independent samples per group) (Insulin stimulation:

639 P=0.0201) (**f**) and AS160 (pT642) (n=4 biologically independent samples per group) (Insulin

640 stimulation: P=0.0726) (**g**). Size markers (in kDa) are shown on illustrative Western blot

641 panels. (**h, i**) Fatty acid composition in triglycerides (TG) (**h**) and phospholipids (PL) (**i**) (n=8

642 biologically independent samples per group). (**j**) mRNA levels of lipogenic enzymes (n=6

643 biologically independent samples per group). Data are mean ±sem. Statistical analysis was

644 performed using two-way ANOVA with Bonferroni's post hoc tests (**a-g**), paired Student's t

645 test (**h, i**) and Wilcoxon's test (**j**). Statistical tests were two-sided. *P<0.05, **P<0.01,

646 ***P<0.001 compared to control.

647

648 **Figure 2.** HSL inhibition is associated with increased insulin sensitivity and adipose tissue

649 ELOVL6 expression *in vivo*. (**a-f**) Experiments were carried out in wild type (WT, white bars)

650 and HSL haploinsufficient (*Lipe*^{+/-}, grey bars) mice. (**a-c**) Glucose infusion rate (GIR) (**a**) post

651 insulin glucose rate of disappearance (Glucose Rd) (**b**) and hepatic glucose production (HGP)

652 (**c**) during euglycemic-hyperinsulinemic clamp in B6D2/F1 mice fed 60% high fat diet for 3

653 months (WT n=7 animals, *Lipe*$^{+/-}$ n=6 animals). (**d**) Plasma glucose concentration during an

654 insulin tolerance test in B6D2/F1 mice fed 45% high fat diet for 3 months (n=12 animals per

655 group). (**e**) QUICKI and (**f**) mRNA level of *Elovl6* in response to refeeding in gonadal

656 adipose tissue (n=8 animals per group) in C57BL/6J mice fed 60% high fat diet for 3 months

657 (n=8 animals per group). (**g-j**) Experiments were carried out in wild type (WT, white bars)

658 and in mice with zinc finger nuclease-mediated deletion of *Lipe* exon B which promoter

659 drives HSL expression in fat cells (*Lipe*$^{exonB-/-}$, grey bars). (**g**) mRNA levels of transcripts

660 containing different exons encoding HSL in inguinal adipose tissue (n=12 animals per group).

661 (**h**) Western blot analysis of adipose tissue HSL protein content (10 μg total protein) (WT n=7

662 animals; *Lipe*$^{exonB-/-}$ n =5 animals). GAPDH was used as Western blot loading control. Size

663 markers (in kDa) are shown on illustrative Western blot panel. (**i**) Plasma glucose

664 concentration and area under the curve (AUC) during a glucose tolerance test (WT n=7

665 animals, *Lipe*$^{exonB-/-}$ n=5 animals) in mice fed 60% high fat diet for 3 weeks and (**j**) mRNA

666 level of adipose tissue *Elovl6* (WT n=5 animals, *Lipe*$^{exonB-/-}$ n=6 animals). Data are mean

667 ±sem. Statistical analysis was performed using Mann and Whitney's test (**a-c**, **h-j**), unpaired

668 Student's t test (**e-g**) or two-way ANOVA with Bonferroni's post-hoc tests (**d**). Statistical

669 tests were two-sided. *P<0.05 compared to control.

670

671 **Figure 3.** ELOVL6 has a positive effect on insulin signaling in adipocytes. (**a, b**) Experiments

672 were carried out in control (white bars, siCTR), single HSL (grey bars, siHSL), single

673 ELOVL6 (light orange bars, siELOVL6) or dual HSL/ELOVL6-deprived (dark orange bars,

674 siHSL/siELOVL6) hMADS adipocytes in basal (-) and insulin-stimulated (+, 100nM)

675 conditions. Insulin signaling evaluated by activating phosphorylation of IRS1 (pY612) (n=7

676   biologically independent samples per group) (Insulin stimulation: P=0.0238) (**a**) and AKT

677   (pS473) (n=7 biologically independent samples per group) (Insulin stimulation: P<0.0001)

678   (**b**). (**c**) Insulin signaling evaluated by activating phosphorylation of AKT (pS473) in wild

679   type (WT, white bars, n=4 animals) and *Elovl6* null (*Elovl6*-/-, light orange bars, n=3 animals)

680   mice injected with a bolus of insulin (Insulin stimulation: P<0.0001). Size markers (in kDa)

681   are shown on illustrative Western blot panels. (**d, e**) Plasma glucose concentration during an

682   insulin tolerance test (n=9 animals per group) (**d**) and gonadal adipose tissue *Elovl6* mRNA

683   levels in response to refeeding (**e**) in DBA/2J (white bars, n=6 animals) and C57Bl/6J (light

684   green bars, n=5 animals) mice. (**f, g**) Glucose disposal rate (GDR) (**f**) and mRNA level of

685   *ELOVL6* in visceral adipose tissue (**g**) from lean healthy (LE, white bars, n=13 individuals)

686   and obese women with metabolic syndrome (MS, light red bars, n=15 individuals). (**h, i**) M-

687   value (**h**) and normalized *ELOVL6* mRNA level (**i**) in subcutaneous adipose tissue of obese

688   women before and two years after bariatric surgery (n=14 individuals). Data are mean ±sem.

689   Statistical analysis was performed using paired (**a, b, d**) and unpaired (**c**) two way ANOVA

690   with Bonferroni's post hoc tests, unpaired Student's t test (**f**), Mann and Whitney's test (**e, g**),

691   and Wilcoxon's test (**h, i**). Statistical tests were two-sided. *P<0.05, **P<0.01, ***P<0.001

692   compared to control condition or other mouse strain. In cell experiments, $^{\$\$}$P<0.01,

693    $^{\$\$\$}$P<0.001 compared to HSL-deprived adipocytes.

694

695   **Figure 4.** Oleic acid content in PL and plasma membrane fluidity mediates ELOVL6 positive

696   effect on insulin signaling. (**a-h**) Experiments were carried out in control (white bars, siCTR),

697   single HSL (grey bars, siHSL), single ELOVL6 (light orange bars, siELOVL6) or dual

698   HSL/ELOVL6-deprived (dark orange bars, siHSL/siELOVL6) hMADS adipocytes. (**a, b**)

699   Fatty acid composition in TG (**a**) and PL (**b**) (n=6 biologically independent samples per

700   group). (**c-f**) hMADS adipocytes were treated with vehicle (DMSO), 1µM of ELOVL6

inhibitor (ELOVL6i) or 75nM of SCD inhibitor (SCDi) for 48h. Fatty acid ratios (n=6 for ELOVL6i and n=5 for SCDi biologically independent samples per group) (**c,e**) and insulin signaling evaluated by activating phosphorylation of AKT (pS473) in basal (-) and insulin-stimulated conditions (+,100nM) (n=4 biologically independent samples per group for ELOVL6i and SCDi) (Insulin stimulation: P<0.0001) (**d,f**). DMSO-treated adipocyte values are common to panels **d** and **f** and, **Supplementary Fig. 1e**. (**g, h**) hMADS were treated with vehicle (V), 100μM (O100) or 500μM (O500) of oleic acid for 48h. Oleic acid levels in PL (n=5 biologically independent samples per group) (**g**) and insulin signaling evaluated by activating phosphorylation of AKT (pS473) (n=5 biologically independent samples per group) in basal (-) or insulin-stimulated (+, 100nM) conditions (Insulin stimulation: P=0.0003) (**h**). For panels **d**, **f** and **h**, cropped images of vehicle and treatment lanes originate from the same blot. Size markers (in kDa) are shown on illustrative Western blot panels. (**i-l**) Experiments were carried out in control hMADS adipocytes expressing green fluorescent protein (GFP) (white bars, Adeno-CTR) or overexpressing human ELOVL6 and GFP (avocado bars, Adeno-ELOVL6). (**i, j**) Fatty acid ratio (n=8 biologically independent samples per group) (**i**) and activating phosphorylation of IRS1 (pY612) in basal (-) and insulin-stimulated conditions (+, 100nM) (n=8 biologically independent samples per group) (Insulin stimulation: P<0.0001) (**j**). (**k, l**) FRAP experiments using fluorescent cholera toxin B (Alexa555-CTxB) (n=5 independent experiments). (**k**) Representative confocal microscope image showing GFP and Alexa455-CTxB at room temperature of a successfully transduced hMADS adipocyte. Scale bar, 50μm. (**l**) Calculated mobile fraction (white bar, n=17 analyzed cells; avocado bar, n=16 analyzed cells). Data are mean ±sem. Statistical analysis was performed using Wilcoxon's test (**a,b**), paired (**c-f**, **h**, **j**) and unpaired (**d**) two way ANOVA with Bonferroni's post hoc tests, Friedman's with Dunn's post hoc tests (**g**), paired Student's t test (**i**) and Mann and Whitney's test (**l**). Statistical tests were two-sided. *P<0.05, **P<0.01, ***P<0.001 compared to control.

726 $^{\$\$}$P<0.01, $^{\$\$\$}$P<0.001 compared to HSL-deprived adipocytes. $^{\#}$P<0.05, $^{\#\#}$P<0.01 compared to

727 HSL- and ELOVL6-deprived adipocytes.

728

729 **Figure 5.** The glucose-sensitive transcription factor, ChREBP, mediates the beneficial effect

730 of diminished HSL expression on glucose metabolism and insulin signaling in adipocytes. (**a-**

731 **e**) Experiments were carried out in control (white bars, siCTR), single HSL (grey bars,

732 siHSL), single ChREBP (light brown bars, siChREBP) or dual HSL/ChREBP-deprived (dark

733 brown bars, siHSL/siChREBP) hMADS adipocytes in basal (**-**) and insulin-stimulated (**+**,

734 100nM) conditions. (**a**) Glucose transport using radiolabelled 2-deoxyglucose (n=12

735 biologically independent samples per group) (Insulin stimulation: P<0.0001). (**b, c**) *de novo*

736 lipogenesis using radiolabelled glucose (n=9 biologically independent samples per group)

737 (Insulin stimulation: P=0.0002) (**b**) or radiolabelled acetate (n=6 biologically independent

738 samples per group) (Insulin stimulation: P=0.0014) (**c**). (**d, e**) Insulin signaling evaluated by

739 activating phosphorylation of IRS1 (pY612) (n=8 biologically independent samples per

740 group) (Insulin stimulation: P=0.0245) (**d**) and AKT (pS473) (n=8 biologically independent

741 samples per group) (Insulin stimulation: P<0.0001) (**e**). Size markers (in kDa) are shown on

742 illustrative Western blot panels. (**f-h**) Experiments were carried out in control (white bars,

743 siCTR) and ChREBP-deprived (light brown bars, siChREBP) hMADS adipocytes. (**f, g**) Fatty

744 acid composition in TG (**f**) and PL (**g**) (n=8 biologically independent samples per group). (**h**)

745 mRNA levels of lipogenic enzymes (n=6 biologically independent samples per group). (**i**)

746 mRNA levels of lipogenic enzymes in inguinal adipose tissue of wild type (WT, white bars,

747 n=7 animals) and *ChREBP* null mice (*Mlxipl*-/-, light brown bars, n=6 animals). (**j,k**)

748 Experiments were carried out in control (white bars, siCTR) and HSL-deprived (grey bars,

749 siHSL) hMADS adipocytes. (**j**) Induction of mRNA levels of *ChREBPα* and *ChREBPβ* (n=8

750 biologically independent samples per group) and (**k**) ChREBP recruitment on *ELOVL6*

751 ChoRE (n=3 independent experiments). (**l, m**) Correlations between mRNA levels of

752 *ELOVL6* and *ChREBPβ* in hMADS adipocytes (n=64 biologically independent samples) (**l**)

753 and in human subcutaneous adipose tissue (n=31 individuals) (**m**). (**n, o**) mRNA levels of

754 *ChREBPβ* (n=7 biologically independent samples per group) (**n**) and *ELOVL6* (n=7

755 biologically independent samples per group) (**o**) in human subcutaneous adipose tissue in

756 basal condition or during hyperglycemic-hyperinsulinemic clamp. Data are mean ±sem.

757 Statistical analysis was performed using paired two way ANOVA with Bonferroni post hoc

758 tests (**a-e**), paired Student's t test (**f, g, j**), Wilcoxon's test (**h, n, o**), Mann and Whitney's test

759 (**i**) and linear regression (**l, m**). Statistical tests were two-sided. *P<0.05, **P<0.01,

760 ***P<0.001 compared to control. $P<0.05, $$P<0.01, $$$P<0.001 compared to HSL-deprived

761 adipocytes. #P<0.05, ##P<0.01 compared to ChREBP-deprived adipocytes.

762

763 **Figure 6.** HSL inhibits ChREBP activity through protein-protein interaction. (**a**)

764 Representative image of immunocomplexes between immobilized FLAG-ChREBPα and

765 recombinant HSL (Rec.HSL) (n=3 independent experiments). (**b**) Representative surface

766 plasmon resonance assay sensorgram showing the binding of HSL to ChREBP. Purified

767 ChREBP (220RU) was first injected on a sensorchip with immobilized anti-ChREBP

768 antibody. Following ChREBP binding, PR65α (no signal) and HSL (35RU) were

769 consecutively injected (n=3 independent experiments). (**c**) Endogenous interaction between

770 HSL and ChREBP in human adipocytes (n=3 biologically independent samples per group).

771 Anti-ChREBP antibody was used for immunoprecipitation (IP). Normal Rabbit IgG antibody

772 was used as negative control. (**d**) Endogenous interaction between HSL and ChREBP in white

773 adipose tissue of *Lipe*^{+/-} (+/-) and wild type (+/+) mice (n=4 animals per group). Anti-

774 ChREBP antibody was used for immunoprecipitation. Rabbit IgG antibody was used as

775 negative control. β-actin was used as Western blot loading control. (**e**) In situ proximity

ligation assays (red signals) performed with anti-HSL and anti-ChREBP antibodies (PLA

HSL/ChREBP) and corresponding image under visible light (Phase) in control (siCTR) and

HSL-deprived (siHSL) hMADS adipocytes. Nuclei were labelled in blue using DAPI.

Representative image (6 independent experiments). Scale bars, 50μm. (**f**) Immunodetection of

ChREBP (red) in control (siCTR) and HSL-deprived (siHSL) hMADS adipocytes.

Representative image (4 independent experiments). Nuclei were labelled in blue using DAPI.

Scale bars, 50μm. (**g**) ChREBPα protein levels in nuclear extracts from control (siCTR) and

HSL-deprived (siHSL) hMADS adipocytes (n=8 biologically independent samples per

group). (**h**) ChREBPα protein levels in nuclear extracts from white adipose tissue of wild type

(WT, n=8 animals) and *Lipe*$^{+/-}$ (n=9 animals) mice. (**i**) Luciferase assays following

transfection in HEK-293 cells of carbohydrate-responsive elements (ChoRE) fused to the

luciferase gene along with expression vectors for ChREBP and HSL. ChoRE activity was

measured in HEK-293 cells transfected with empty plasmid (pcDNA), ChREBP and different

concentrations of HSL expression plasmids under low (5mM, G5) (n=6 biologically

independent samples per group) and high (25mM, G25) glucose concentrations (n=4

biologically independent samples per group). (**j**) HSL and ChREBPα immunocomplexes in

HEK-293 cells transfected with empty plasmid (pcDNA3), FLAG-ChREBP, full lengh HSL

(HSL) or short form HSL (HSL-S) expression plasmids. Anti-FLAG antibody was used for

immunoprecipitation. β-actin was used as Western blot loading control (n=3 independent

experiments) (**k,l**) Effect of overexpression of the short inactive form of HSL (HSL-S) in

hMADS adipocytes. Experiments were carried out in control (siCTR, white bars) and HSL-

deprived (siHSL, grey bars) hMADS adipocytes overexpressing green fluorescent protein

(GFP, Ad-CTR) or the short inactive form of HSL (Ad-HSL-S). (**k**) mRNA levels of *ELOVL6*

(n=10 biologically independent samples per group). (**l**) Activating phosphorylation of IRS1

(pY612) in basal (-) and insulin-stimulated (+, 100nM) conditions (n=6 biologically

801   independent samples per group, Insulin stimulation: $P<0.0001$). Size markers (in kDa) are

802   shown on illustrative Western blot panels. Data are mean ± sem. Statistical analysis was

803   performed using paired Student's t test (**g**), Mann and Whitney's test (**h**) or paired two-way

804   ANOVA with Bonferroni's post-hoc tests (**i, k, l**). Statistical tests were two-sided. *$P<0.05$,

805   **$P<0.01$ ***$P<0.001$ compared to ChREBP condition (**i**) or control adipocyte (**l**). $P<0.05$,

806     $$$$P<0.001$ compared to pcDNA condition (**i**) or siHSL/Ad-CTR adipocytes (**k, l**).

807

808   METHODS

809   **General experimental approaches.** No samples, mice, human research participants and data

810   points were excluded from the reported analysis. Randomization was not performed. Analyses

811   were not blinded except when noted below. Detailed information and description of common

812   techniques are described in Supplementary Methods as indicated below.

813   **Culture of human adipocytes and in vitro measurements.**

814   Culture of adipocytes. hMADS cells were expanded in DMEM 5.5 mM glucose (Lonza)

815   supplemented with 10% fetal bovine serum (Lonza), 2 mM L-glutamine (Invitrogen), 10 mM

816   HEPES buffer (Lonza), 50 units/ml of penicillin (Invitrogen), 50 mg/ml of streptomycin

817   (Invitrogen), supplemented with 2.5 ng/ml of fibroblast growth factor 2 (Sigma). At

818   confluence, fibroblast growth factor 2 was removed from proliferation medium. On the next

819   day (day 0), the cells were incubated in differentiation medium (DMEM/Ham's F-12 medium

820   containing 7.8 mM glucose, HEPES, L-glutamine, penicillin/streptomycin, 10 µg/ml of

821   transferrin (Sigma), 10nM of insulin (Sigma), 0,2 nM triiodothyronine (Sigma), 100 µM 3-

822   isobutyl-1-methylxanthine (Sigma), 1 µM dexamethasone (Sigma), and 100 nM rosiglitazone

823   (Sigma)). At days 3 and 10, respectively, dexamethasone and 3-isobutyl-1-methylxanthine,

824   and then rosiglitazone were removed from culture medium. The experiments were carried out

825   between days 12 and 15.

826   For primary culture and differentiation of human preadipocytes, subcutaneous adipose tissue

827   samples were obtained from 5 women (age 39 ± 9 years; BMI 28 ± 4 kg/m^2) undergoing

828   elective plastic surgery in the abdominal or dorsal region at Rangueil Hospital, Toulouse,

829   France. Adipose tissue was cleaned from blood vessels and fibrous material, minced into

830   pieces and digested in 1 volume of collagenase I (300 units/ml, Sigma) for 90 min in 37 °C

831   shaking water bath. Digested tissue was filtered through 250 µm strainer, diluted with

832   PBS/gentamycin and centrifuged at 1300 rpm for 5 min. Pellet was incubated in erythrocyte

833 lysis buffer for 10 min at room temperature. Cells were filtered, centrifuged, resuspended in

834 PM4 medium with 132 nmol/L insulin for differentiation and collected at day 13 [51,52]. The

835 study was approved by the Ethics Committee of Toulouse University Hospitals (Comité de

836 Protection des Personnes Sud Ouest et Outre Mer 2, DC-2014-2039). The volunteers signed

837 informed consent for anonymous use of samples.

838 HEK293 and HepG2 cell cultures. See Supplementary Methods.

839 RNA interference. RNA interference was achieved by small interfering RNA (siRNA).

840 Briefly, on day 7 and day 4 of differentiation respectively, hMADS and primary

841 preadipocytes were detached from culture dishes with trypsin/EDTA (Invitrogen) and

842 counted. Control small interfering RNA against Green Fluorescent Protein (siCTR) and gene-

843 specific siRNA for HSL, ChREBP, ELOVL6 and ATGL (Eurogentec) were delivered into

844 adipocytes using a microporator (Invitrogen) with the following parameters: 1,100 V, 20 ms,

845 1 pulse. The targeted sequences are provided in Supplementary Methods.

846 Adenoviral infection. Adenoviruses encoding under the control of a cytomegalovirus

847 promoter, ELOVL6 (ADV-207862), the short form of HSL, both in tandem with GFP, or GFP

848 alone (catalog No. 1060) were obtained from Vector Biolabs. Adenoviral particles

849 (multiplicity of infection, 200) were added in the culture medium for 24 hours at day 11-12 of

850 hMADS cell differentiation. Medium was changed and experiments were carried out 48 hours

851 later.

852 Plasmid transfection. See Supplementary Methods.

853 Oleic acid supplementation in human adipocytes. See Supplementary Methods.

854 Treatments with enzyme inhibitors. For FAS, SCD and ELOVL6 inhibition, hMADS

855 adipocytes were respectively treated with 1µM of compound AZ12756122 (ex 117 from

856 WO2008075070A1, synthesized at AstraZeneca), 75nM of A939572 [24] (Tocris Biosciences)

857 and 1w [23] (provided by AstraZeneca) in culture medium for 48 hours. To study the effect of

858   bioactive FA on the induction of ChREBP, cells were treated for 8h with 10μM of triacsin C

859   (Sigma), an inhibitor of acyl-CoA synthase, in the culture medium.

860   Gene expression analysis. See Supplementary Methods.

861   Characterization of human ChREBPβ-specific exon. See Supplementary Methods.

862   Western blot analysis. See Supplementary Methods.

863   Metabolic measurements. Triacylglycerol hydrolase activity was measured on cell extracts [14].

864   For other metabolic measurements, insulin was removed from culture medium the day before

865   the assay. To determine glucose uptake, cells were incubated 50 min at 37°C with or without

866   100 nM insulin. Then, 125 μM of cold 2-deoxy-Dglucose and 0.4 μCi 2-deoxy-D-[^{3}H]

867   glucose (Perkin Elmer) per well were added for 10 min incubation. Culture plates were put on

868   ice and rinsed with 10 mM glucose in ice-cold PBS and then with ice-cold PBS. Cells were

869   scraped in 0.05N NaOH, and radioactive 2-deoxy-D-glucose uptake was measured by liquid

870   scintillation counting of cell lysate. To determine glucose oxidation, cells were incubated for

871   3 h in Krebs Ringer buffer supplemented with 2% BSA, 10 mM HEPES, 2 mM glucose, and

872   1 μCi D-[^{14}C(U)]glucose (PerkinElmer) with or without 100 nM insulin. A 2x2 cm Whatman

873   3M paper was placed on top of each well and soaked with 120 μL NaOH 1N. After

874   incubation, filter-trapped $^{14}CO_2$ was measured by liquid scintillation counting. Medium was

875   acidified with 1M sulfuric acid and medium $^{14}CO_2$ was trapped by benzethonium hydroxide,

876   during 2 h incubation. Benzethonium-trapped $^{14}CO_2$ was measured by liquid scintillation

877   counting. Specific activity was counted and used to determine the quantity of oxidized

878   glucose equivalent. To assess glucose incorporation into FA, cells were then washed twice in

879   PBS and then scraped in STED. Neutral lipids were extracted in methanol/chloroform (1:2).

880   Organic phase was dried under nitrogen and hydrolyzed in 1mL 0.25N NaOH in

881   methanol/chloroform (1:1) for 1 h at 37°C. The solution was neutralized with 500 μL 0.5N

882   HCl in methanol. FAs and glycerol were separated by adding 1.7 mL chloroform, 860 μL

883   water, and 1 mL methanol/chloroform (1:2). Incorporation of ^{14}C into FAs was measured by

884   liquid scintillation counting of the lower phase. Specific activity was counted and used to

885   determine the quantity of incorporated glucose equivalent. *De novo* lipogenesis was also

886   measured using acetic acid-sodium salt-[1-^{14}C] (PerkinElmer). Cells were incubated for 3h in

887   Krebs buffer supplemented with 10mM HEPES, 2mM glucose, 2%BSA and 2μCi/mL of

888   radiolabelled acetate stimulated with or without 100nM insulin. Cells were then washed twice

889   and harvest in PBS/SDS 0.1%. Neutral lipids were extracted in methanol/chloroform (1:2)

890   method. Incorporation of ^{14}C into neutral lipids was measured by liquid scintillation counting

891   of lower phase. Results from metabolic measurements were normalized to total protein

892   content of cell extracts.

893   ELOVL6 activity. Fatty acid elongation activity was measured in crude microsomal extracts

894   from hMADS adipocytes [41]. Briefly, cells were washed with PBS, scraped in 3 ml of ice-cold

895   250m M sucrose, Hepes 20 mM, EDTA 1 mM, pH 7.5 and dounce-homogenized.

896   Homogenate was centrifuged 1000 g at 4°C for 7 min. Supernatant was collected and

897   centrifuged at 2000 g at 4°C for 30 min. Supernatant was collected and centrifuged at 17000 g

898   at 4°C for 1 hour. The resultant pellet was suspended in 50 μl of 100 mM Tris-HCl, pH 7.4

899   and used for fatty acid elongation activity after determination of protein concentration.

900   ELOVL6 activity was essayed by the measurement of [2-^{14}C]malonyl-CoA (Perkin Elmer)

901   incorporation into exogenous palmitoyl-CoA [53]. ELOVL6 inhibitor (1μM of compound 1w [23])

902   was preincubated 30 min at 37°C with microsomal protein before addition of reaction

903   mixture. Incubation was stopped by adding 0.2 ml of 5M KOH, 10% methanol and saponified

904   at 65°C for 1h. Then the samples were cooled and acidified with 0.2 ml of ice-cold 5N HCl

905   and 0.2 ml of ethanol. Free fatty acids were extracted from the mixture three times with 1 ml

906   of hexane, 2% acetic acid. The pooled hexane fractions were dried under nitrogen and after

907   addition of 3 ml of scintillation cocktail, the radioactivity incorporated was counted. Blanks

908   were carried out in parallel reactions incubated without microsomal fractions. ELOVL6

909   activity obtained by subtracting [^{14}C]malonyl-CoA molecules incorporated into fatty acids in

910   the absence of inhibitor to the values in the presence of the ELOVL6 inhibitor.

911   Chromatin immunoprecipitation assays. Human adipocyte cells (10^7 cells per condition) were

912   fixed with 1% formaldehyde for 15 min and quenched with 0.125 M glycine. Chromatin was

913   isolated by the addition of lysis buffer, followed by disruption with a Dounce homogenizer.

914   Lysates were sonicated and the DNA sheared to an average length of 300-500 bp. Genomic

915   DNA (Input) was prepared by treating aliquots of chromatin with RNase, proteinase K and

916   heat for de-crosslinking, followed by ethanol precipitation (Active Motif Inc.). Pellets were

917   resuspended and the resulting DNA was quantified on a NanoDrop spectrophotometer.

918   Extrapolation to the original chromatin volume allowed quantitation of the total chromatin

919   yield. Aliquots of chromatin (30 µg) were precleared with protein A agarose beads

920   (Invitrogen). Genomic DNA regions of interest were isolated using an antibody against

921   ChREBP (Novus, cat# NB400-135). Positive and negative controls were designed by Active

922   Motif Inc. Complexes were washed, eluted from the beads with SDS buffer, and subjected to

923   RNase and proteinase K treatment. Crosslinks were reversed by incubation overnight at 65 C,

924   and ChIP DNA was purified by phenol-chloroform extraction and ethanol precipitation.

925   Quantitative PCR reactions were carried out in triplicate using SYBR Green Supermix (Bio-

926   Rad, Cat # 170-8882) on a CFX Connect™ Real Time PCR system. Positive and negative

927   control sites were tested for each factor as well as the sites of interest. The resulting signals

928   were normalized for primer efficiency by carrying out qPCR for each primer pair using input

929   DNA (pooled unprecipitated genomic DNA from each sample).

930   Cellular subfractionation. Nuclear and cytosolic fractions from hMADS adipocytes were

931   prepared using Nuclear Extract Kit (40010) from Active Motif. Cells were rinsed with PBS

932   and immediately scrapped into 1X Hypotonic Buffer. For adipose tissue, tissues were ground

933 in liquid nitrogen and lysed using the NE-PER nuclear and cytoplasmic extraction reagent kit

934 (Thermoscientific, 78835). Subsequent steps followed the manufacturer's protocol. Anti-

935 histone H3 (4499, Cell Signaling Technology), anti-lamin A/C (4777, Cell Signaling

936 Technology) and α tubulin (T5168, Sigma) antibodies were used to analyze the efficiency of

937 cellular fractionation.

938 Fatty acid composition of TG and PL. Cells were scraped in PBS and then mixed with

939 methanol supplemented with butylated hydroxytoluene (BHT) 0.001%. Lipid extraction was

940 performed with a chloroform/methanol mixture (1:1) and KCl (0.5 M) after centrifugation

941 (2500rpm, 10min). PL and TG were isolated by thin-layer chromatography on silica glass

942 plates (Merck) using petroleum ether/diethyl ether/acetic acid (80:20:1) as the mobile phase.

943 FA methyl esters were generated by transmethylation of the glycerolipids in methanol with 5

944 % acetyl chloride at 60°C for 1 hour, extracted 2 times by isooctane. Analysis was carried out

945 with a gas chromatograph (Shimadzu GC 2100) equipped with a CP-Wax 58 capillary

946 column, 50 m in length, 0.25-mm external diameter and 0.2-μm thickness of the stationary

947 phase (Varian Inc.), with helium 1 mL/min as carrier gas. Programmed temperature

948 vaporization (PTV system) injector and flame ionization detector were used. Results are

949 expressed in percentage of total FA contained in the sample.

950 Fatty acid composition in phospholipid classes. See Supplementary Methods.

951 Measurement of glycerol and NEFA in culture medium. See Supplementary Methods.

952 Fluorescence recovery after photobleaching (FRAP). Cells were labeled for 15 min with

953 1μg/ml Alexa 555-labeled Cholera ToxinSubunit B (CTxB Molecular Probes) at 4°C, then

954 washed three times in chilled medium supplemented with 25 mM HEPES buffer, pH 7.4.

955 LSM780 confocal microscope, equipped with a high sensitive 32 channel GaAsP detectors,

956 operated with Zen Black software, coupled to a DPSS-laser (561 nm, maximum power 20

957 mW) was used for excitation with a detection bandwidth of 571-624 nm (Carl Zeiss). All

958   experiments were done at room temperature (22°C). Cells were observed using a Plan-

959   Apochromat 63X NA 1.4 oil immersion objective, and the pixel dwell was set to the optimal

960   value of 1.92 μs. The fluorescence intensity of three regions of interest of 6.4 μm×3.2 μm was

961   measured: the photobleached area, a region within the cell that was not photobleached to

962   check for overall photobleaching and cell position fluctuation and the background. After 10

963   prebleach scans (one scan every 200 ms) at 1% maximal laser power to determine initial

964   fluorescence intensity, one photobleaching scan was performed at 100% laser power. Post

965   bleach fluorescence recovery was then sampled at 1% laser power for 150 s. FRAP data

966   analysis was done using the method described by Bonneau *et al.* [54].

967   Immunoprecipitation. HEK293T cells were harvested in a lysis buffer containing 3% NaCl

968   5M, 5% TrisHCl 1M (pH 7.5), 1% EDTA 500mM, 1.338% PPiNa and 0.02% NaF,

969   supplemented with 1% Triton X-100 (Sigma), 2% 50X protease inhibitor cocktail (Roche)

970   and 1% 1mM orthovanadate (Sigma). 1 mg of proteins was immunoprecipitated overnight at

971   4°C, with 40μL of anti-FLAG M2 magnetic beads (Sigma). Beads were gently centrifuged for

972   1 min and washed with the lysis buffer before elution in Laemmli buffer.

973   For immunoprecipitation between purified proteins, FLAG-tagged ChREBP was expressed in

974   HEK293T cells. Cells were harvested in lysis buffer described above. 300 μg of proteins was

975   immunoprecipitated overnight at 4°C with 40μL of anti-FLAG M2 magnetic beads. Beads

976   bound with ChREBP were washed with the lysis buffer and incubated with 1 μg of human

977   recombinant HSL (Cayman) in 350 μl of lysis buffer for 3h at 4 °C with gentle rocking. The

978   beads were washed 3 times with lysis buffer.

979   For endogenous co-immunoprecipitation in hMADS adipocytes, cells were lysed for 15min in

980   1X hypotonic buffer (Active Motif) with 4% 25X protease inhibitor cocktail (Roche) and

981   1mM orthovanadate (Sigma). Cell debris and fat was discarded after 12700rpm centrifugation

982   at 4°C for 15min. Preclearing was performed at 4°C for 30min using 50μL protein G and 4μg

983   control rabbit (2729, Cell Signaling Technology) or mouse (sc-2025, Santa Cruz) IgG. Beads

984   were discarded and supernatants were incubated with 4μg anti-ChREBP (NB400-135, Novus)

985   ou 2μg anti-HSL (sc-74489, Santa Cruz Biotechnology) for 90 min at 4°C. As negative

986   control of immunoprecipitation, 4μg control rabbit (2729, Cell Signaling Technology) or 2μg

987   mouse (sc-2025, Santa Cruz) IgG were used. Protein A/protein G (50:50) magnetic beads

988   were added for 1h at 4°C. Beads were washed in cold PBS with 4% 25X EDTA and 1mM

989   orthovanadate.

990   For ChREBP immunoprecipitation in mouse white adipose tissue, fat was cut in small pieces

991   and lysed during 2h in 20 mM Tris/HCl, 150 mM NaCl, 0.5% NP-40 and

992   protease/phosphatase inhibitors; pH 8. Following centrifugation at 15000g for 20 min at 4°C,

993   fat layer was removed before collecting the supernatant. For each immunoprecipitation, 0.8 to

994   1 mg of protein was precleared with 50 μl of Protein A Dynabeads (ThermoFisher) for 1h at

995   4°C, then incubated overnight at 4°C with 40μl Protein A dynabeads coupled with 5μg Rabbit

996   IgG or ChREBP antibody (Novus). Beads were washed 4 time with lysis buffer prior elution

997   in 2X Laemmli buffer.

998   In situ proximity ligation assay and immunofluorescence. In situ proximity ligation assay was

999   performed using Duolink In Situ reagents (Sigma). Cells and pieces of subcutaneous adipose

1000   tissue were fixed with 4% paraformaldehyde (Sigma) and permeabilized 15 min at room

1001   temperature with 0.2% Triton X-100 (Sigma). Incubation of antibodies, ligation of

1002   oligodeoxynucleotides and amplification were performed following manufacturer's

1003   instructions. The following primary antibodies were incubated overnight at 4°C: anti-HSL

1004   (murine antibody, sc-74489, Santa Cruz Biotechnology), anti-ATGL (mouse antibody, NBP2-

1005   59390, Novus), anti-AKT (mouse antibody, 2920, Cell Signaling Technology) and anti-

1006   ChREBP (rabbit antibody, NB400-135, Novus). The same antibodies were used in

1007   immunofluorescence assays. Anti-mouse (Alexa-fluor 488-conjugated, A21202, and Alexa-

1008   fluor 546-conjugated, A10036, Invitrogen) and anti-rabbit (Alexa-fluor 546-conjugated,

1009   Invitrogen) secondary antibodies were incubated at 1/300 for 45min. Neutral lipids were

1010   stained using Bodipy (4-3922, Life Technologies) for 30min. Nucleus labeling was performed

1011   using Hoescht (33342, 5mg/mL, Invitrogen) for 5 min. Confocal microscopy was performed

1012   using Zeiss LSM780. Image processing was similar for all conditions. The same settings were

1013   applied to entire images.

1014   Surface Plasmon Resonance assays. All binding studies based on surface plasmon resonance

1015   technology were performed on BIAcore T200 optical biosensor instrument (GE Healthcare).

1016   Immobilization of anti-ChREBP antibody (NB400-135, Novus) was performed by the Fc

1017   region to the chip surface using native Protein A sensorchip in PBS-P+ buffer (20mM

1018   Phosphate Buffer pH 7.4, 2.7mM Kcl, 137mM NaCl, and 0.05% surfactant P20) (GE

1019   Healthcare). Immobilization step were performed at a flow rate of 5 µl/min with a final

1020   concentration of 2µg/ml. Total amount of immobilized antibody was 11000-12000RU. Then

1021   all injection steps were performed at a flow rate of 20µl/min.Channel Fc1 was used as a

1022   reference surface for non-specific binding measurements.

1023   Luciferase activity. See Supplementary Methods.

1024

1025   **Animal studies.** No randomization and blinding was performed. Animals from several litters

1026   were used in each protocol to avoid litter-to-litter variation.

1027   Mouse models. Targeted disruption of the *Lipe* gene and generation of *Lipe*$^{+/-}$ mice have been

1028   described elsewhere [13]. Before euthanasia, mice were fasted for 24h or refed for 18h

1029   supplemented with 20% glucose in drinking water. To create transgenic mice with specific

1030   deletion of *Lipe* exon B, mRNA coding for zinc finger nucleases targeting specifically HSL

1031   (CompoZr™ Custom Zinc Finger Nucleases, CSTZFN-1KT, Sigma) was injected into

1032   pronuclei of one-cell embryos from female B6D2/F1 mice. Homozygous mice (*Lipe*$^{exonB-/-}$

1033   registered as B6D2-*Lipe^em1Land* mice) were obtained. Full description of the model will be

1034   published elsewhere. The specific inhibitor of HSL (BAY 59-9435) was synthesized by

1035   NoValix (Illkirch, France) [55]. Transgenic mice were fed high fat diet (60% or 45% kcal fat,

1036   respectively, D12492 and D12451 from Research Diets) for indicated times. In

1037   pharmacological studies, C57BL/6J male mice (12-15 weeks-old, Janvier Laboratories) were

1038   treated orally with DMSO or HSL inhibitor (70mg/kg once daily) for 11 days. Eight week-old

1039   DBA2/J and C57BL6/J male mice (Charles River) were fed high fat diet (60% kcal fat,

1040   D12492 from Research Diets) for 6 weeks before sacrifice. Mice were housed and

1041   manipulated according to Inserm guidelines and European Directive 2010/63/UE in the local

1042   animal care facility (agreements A 31 555 04 and C 31 555 07). Protocols were approved by

1043   the French Ministry of Research following review by local ethical committee (CEEA122).

1044   In studies on ChREBP null mice, 10 to 12 week-old male and female *Mlxipl* global knockout

1045   mice [56] and wild-type littermates were maintained in a 12-h light/dark cycle with water and

1046   chow diet (65% carbohydrate, 11% fat, and 24% protein). For fasting-refeeding experiment,

1047   mice were either fasted for 24h (fasted group) or refed for 18h on chow diet and had access to

1048   drinking water with 20% glucose, following a 24h fast (Refed group). Mice were housed and

1049   manipulated according to Inserm guidelines and European Directive 2010/63/UE in the local

1050   animal care facility (agreement A751320). Protocols were approved by the French Ministry of

1051   Research following review by local ethical committee (CEEA34).

1052   Mice homozygous for a deletion in *Elovl6* and their wild-type littermates were phenotyped on

1053   a C56BL6/J background [57]. The research has been regulated under the Animals (Scientific

1054   Procedures) Act 1986 Amendment Regulations 2012 following ethical review by the

1055   University of Cambridge Animal Welfare and Ethical Review Body (AWERB).

1056   Gene and protein expression analyses. See Supplementary Methods.

1057   Measurement of fasting glucose and insulin. See Supplementary Methods.

1058   Glucose and insulin tolerance tests and insulin bolus injection. See Supplementary Methods.

1059   Euglycemic-hyperinsulinemic clamp. See Supplementary Methods.

1060   **Human research.** Nature of the groups was blinded to the investigator performing gene

1061   expression experiments.

1062   Women with differing obese and metabolic status. Participating women (lean group mean age

1063 37 ± 16 years; obese with metabolic syndrome group mean age, 49 ± 11 years) were

1064   scheduled to have abdominal surgery (laparoscopic or laparotomic cholecystectomy and

1065   gastric banding) [58]. During the surgical procedure, samples of visceral adipose tissue were

1066   obtained by surgical excision. Euglycemic hyperinsulinemic clamp was performed at rest

1067   after an overnight fast. Each subject gave written informed consent and the study was

1068   approved by the Ethics Committee of the Third Faculty of Medicine, Charles University,

1069   Prague.

1070   Hyperglycemic hyperinsulinemic clamp. The 8 participating men were 23 ± 3 years-old

1071   (BMI, 23 ± 2 kg/m^2). The hyperglycemic hyperinsulinemic clamp was a modification of the

1072   hyperglycemic method used by Del Prato et al. combined with the original hyperinsulinemic

1073   clamp described by Defronzo [59,60]. For hyperglycemia, the objective was to increase plasma

1074   glucose 5.5 mmol/l above fasting level by infusing 20% dextrose in two phases: 1) bolus dose

1075   to increase glycemia to the desired target and 2) continuous infusion dose adjusted every 5–10

1076   min according to measured plasma glucose to maintain glycemia at the desired target. To

1077   obtain hyperinsulinemia, insulin was co-infused at the rate of 75 mU/m^2·min for 180 min. The

1078   study was approved by the Ethics Committee of University of Montreal. The volunteers gave

1079   their written consent after being informed of the nature, purpose, and possible risks of the

1080   study.

1081   Morbidly obese subjects undergoing bariatric surgery. This cohort has in part been described

1082   before [61]. In brief, 14 obese women (BMI>35 kg/m^2; age, 48 ± 9 years) referred to the

1083   hospital for gastric by-pass surgery (Roux-en-Y) were investigated before surgery and 2 years

1084   post-operatively. According to self-report, body weight had been stable (± 2 kg) for at least 3

1085   months prior to both investigations. The study was approved by the regional ethics board in

1086   Stockholm and registered at clinicaltrials.gov as NCT01785134. Subjects were randomized to

1087   omentectomy or not and this was blinded to investigators and patients. Procedure was

1088   explained in detail to each women and written informed consent was obtained.

1089   Gene expression analysis. See Supplementary Methods.

1090

1091   **Statistical analysis.** Results from biological replicates were expressed as mean ± SEM.

1092   Statistical analyses were performed using GraphPad Prism (GraphPad Software v.5.0).

1093   D'Agostino and Pearson omnibus normality test was used to test normality. Fischer test was

1094   used to test for equality of variances. Data were Log transformed when appropriate to reach

1095   normality and uniform distribution. Statistical tests were two-sided. Paired or unpaired

1096   Student's t tests, Wilcoxon's test and, Mann and Whitney's test were performed to compare

1097   two conditions. Paired or unpaired one-way ANOVA and Friedman's tests were performed

1098   and followed respectively by Bonferroni's and Dunn's post hoc tests to determine differences

1099   between several groups. Paired or unpaired two-way ANOVA with Bonferroni's post hoc

1100   tests were used to compare two variables. Linear regression was used to test association

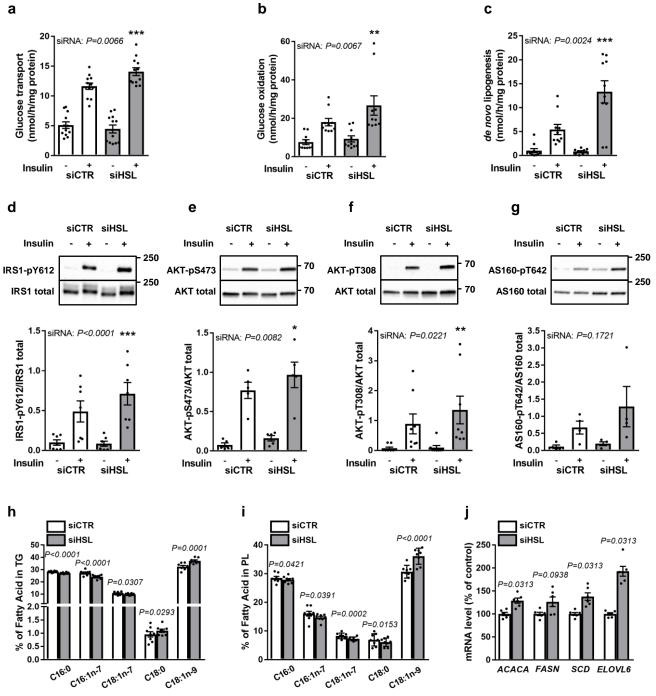1101   between two variables.

1102

1103   **Data availability statement.** The data that support the plots within this paper and other

1104   findings of this study are available from the corresponding author upon reasonable request.
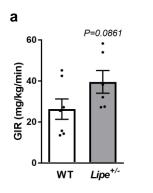
1105

1106   METHODS-ONLY REFERENCES
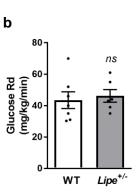
1107   51.   Skurk, T., Ecklebe, S. & Hauner, H. A novel technique to propagate primary human

1108   preadipocytes without loss of differentiation capacity. *Obesity (Silver Spring)* **15**,

1109   2925-2931 (2007).

1110   52.   Rossmeislova, L*., et al.* Weight loss improves the adipogenic capacity of human

1111   preadipocytes and modulates their secretory profile. *Diabetes* **62**, 1990-1995 (2013).

1112   53.   Moon, Y.A., Shah, N.A., Mohapatra, S., Warrington, J.A. & Horton, J.D.

1113   Identification of a mammalian long chain fatty acyl elongase regulated by sterol

1114   regulatory element-binding proteins. *J Biol Chem* **276**, 45358-45366 (2001).

1115   54.   Bonneau, L*., et al.* Plasma membrane sterol complexation, generated by filipin,

1116   triggers signaling responses in tobacco cells. *Biochim Biophys Acta* **1798**, 2150-2159

1117   (2010).

1118   55.   Langin, D*., et al.* Adipocyte lipases and defect of lipolysis in human obesity. *Diabetes*

1119   **54**, 3190-3197 (2005).

1120   56.   Iizuka, K., Bruick, R.K., Liang, G., Horton, J.D. & Uyeda, K. Deficiency of

1121   carbohydrate response element-binding protein (ChREBP) reduces lipogenesis as well

1122   as glycolysis. *Proc Natl Acad Sci U S A* **101**, 7281-7286 (2004).

1123   57.   Tan, C.Y*., et al.* Brown Adipose Tissue Thermogenic Capacity Is Regulated by

1124   Elovl6. *Cell Rep* **13**, 2039-2047 (2015).

1125   58.   Klimcakova, E*., et al.* Worsening of obesity and metabolic status yields similar

1126   molecular adaptations in human subcutaneous and visceral adipose tissue: decreased

1127   metabolism and increased immune response. *J Clin Endocrinol Metab* **96**, E73-82

1128   (2011).

1129   59.   DeFronzo, R.A., Tobin, J.D. & Andres, R. Glucose clamp technique: a method for

1130   quantifying insulin secretion and resistance. *Am J Physiol* **237**, E214-223 (1979).

1131   60.   Del Prato, S*., et al.* Characterization of cellular defects of insulin action in type 2 (non-

1132   insulin-dependent) diabetes mellitus. *J Clin Invest* **91**, 484-494 (1993).

1133   61.   Dahlman, I*., et al.* The fat cell epigenetic signature in post-obese women is

1134   characterized by global hypomethylation and differential DNA methylation of

1135   adipogenesis genes. *Int J Obes (Lond)* **39**, 910-919 (2015).

1136

a

Glucose transport (nmol/h/mg protein)

siRNA: *P=0.0066* ***

Insulin − + − +
siCTR siHSL

b

Glucose oxidation (nmol/h/mg protein)

siRNA: *P=0.0067* **

Insulin − + − +
siCTR siHSL

c

de novo lipogenesis (nmol/h/mg protein)

siRNA: *P=0.0024* ***

Insulin − + − +
siCTR siHSL

d

siCTR siHSL
Insulin − + − +

IRS1-pY612 — 250
IRS1 total — 250

IRS1-pY612/IRS1 total

siRNA: *P<0.0001* ***

Insulin − + − +
siCTR siHSL

e

siCTR siHSL
Insulin − + − +

AKT-pS473 — 70
AKT total — 70

AKT-pS473/AKT total

siRNA: *P=0.0082* *

Insulin − + − +
siCTR siHSL

f

siCTR siHSL
Insulin − + − +

AKT-pT308 — 70
AKT total — 70

AKT-pT308/AKT total

siRNA: *P=0.0221* **

Insulin − + − +
siCTR siHSL

g

siCTR siHSL
Insulin − + − +

AS160-pT642 — 250
AS160 total — 250

AS160-pT642/AS160 total

siRNA: *P=0.1721*

Insulin − + − +
siCTR siHSL

h

% of Fatty Acid in TG

□ siCTR ■ siHSL

P<0.0001 *P<0.0001* *P=0.0307* *P=0.0293* *P=0.0001*

C16:0 C16:1n-7 C18:1n-7 C18:0 C18:1n-9

i

% of Fatty Acid in PL

□ siCTR ■ siHSL

P=0.0421 *P=0.0391* *P=0.0002* *P=0.0153* *P<0.0001*

C16:0 C16:1n-7 C18:1n-7 C18:0 C18:1n-9

j

mRNA level (% of control)

□ siCTR ■ siHSL

P=0.0313 *P=0.0938* *P=0.0313* *P=0.0313*

ACACA *FASN* *SCD* *ELOVL6*

a

siCTR siHSL siELOVL6 siHSL/siELOVL6

Insulin − + − + − + − +

IRS1-pY612 ⟶ 250 / 250

IRS1 total

IRS1-pY612/IRS1 total

siRNA: P=0.0314

** $$ $$

Insulin − + − + − + − +
siCTR siHSL siELOVL6 siHSL/siELOVL6

b

siCTR siHSL siELOVL6 siHSL/siELOVL6

Insulin − + − + − + − +

AKT-pS473 ⟶ 70

AKT total ⟶ 70

AKT-pS473/AKT total

siRNA: P<0.0001

*** $$$ *** $$

Insulin − + − + − + − +
siCTR siHSL siELOVL6 siHSL/siELOVL6

c

WT Elovl6−/−

Insulin − − − + + +   − − − + + +

AKT-pS473 ⟶ 55

AKT total ⟶ 55

AKT-pS473/AKT total

Genotype: P=0.0112

*

Insulin − + − +
WT   Elovl6−/−

d

□ DBA/2J
■ C57BL/6J

Plasma glucose (mg/dl) vs Time (min)

*

Genotype: P=0.0122

e

Elovl6 mRNA level (% of fasting)

P=0.0173

DBA/2J C57BL/6J

f

GDR (mg/kg/min)

P<0.0001

LE MS

g

ELOVL6 mRNA level

P=0.0061

LE MS

h

M-value

P=0.0002

Before After

i

ELOVL6 mRNA level

P=0.0001

Before After

a

FLAG-ChREBP	-	+	+
Rec-HSL	+	+	-
pcDNA	+	-	+

IP: FLAG, WB: HSL — 250

IP: FLAG, WB: FLAG — 130

b

Start ChREBP injection
Stop injection
Start PR65α injection
Stop injection
Stop HSL injection
Start HSL injection
Stop injection

c

Input | IP: ChREBP | IP: IgG

WB: ChREBPα — 130
WB: HSL — 100
WB: ATGL — 70
WB: GAPDH — 40

d

Input | IP: ChREBP

IP: IgG

+/+ -/+

HSL
ChREBPα
β-actin

e

siCTR | siHSL

PLA HSL/ChREBP

PLA+Phase+DAPI

f

siCTR | siHSL

ChREBP

ChREBP + DAPI

g

siCTR | siHSL

ChREBPα — 130
Histone — 17

P=0.0024

siCTR siHSL

ChREBPα/total proteins (nuclear fraction)

h

WT | Lipe+/-

ChREBPα
Lamin A/C

P=0.0150

WT Lipe+/-

ChREBPα/total proteins (nuclear fraction)

i

- pcDNA
- ChREBP
- ChREBP+25ng HSL
- ChREBP+50ng HSL
- ChREBP+100ng HSL
- ChREBP+200ng HSL

Glucose: P<0.0001
Plasmids: P<0.0001

ChoRE activity (luc/βgal)

$$$
**   ***   ***

Glucose 5mM   Glucose 25mM

j

FLAG-ChREBP	-	+	-	-	+	+
HSL	-	-	+	-	+	-
HSL-S	-	-	-	+	-	+
pcDNA	+	+	+	+	-	-

WB: ChREBP — 130
WB: HSL — 95
WB: β-actin — 35
IP: FLAG, WB:HSL — 95

k

siCTR
siHSL

siRNA: P<0.0001
Adeno: P<0.0001

$$$

ELOVL6 mRNA level (% of siCTR-AdCTR)

Ad-CTR Ad-HSL-S Ad-CTR Ad-HSL-S

l

siCTR Ad-CTR | siCTR Ad-HSL-S | siHSL Ad-CTR | siHSL Ad-HSL-S

Insulin - + - + - + - +

IRS1-pY612 — 170
IRS1 total — 170

siCTR
siHSL

siRNA/Adeno: P=0.0087

* $

IRS1-pY612/IRS1 total

Insulin - + - + - + - +

Ad-CTR Ad-HSL-S Ad-CTR Ad-HSL-S